

# Entrapment of a *Pseudo-Tetrahedral* Co<sup>II</sup> Center by Thioether Sulfur Bound {Co<sub>2</sub>( $\mu$ -L)} Fragments: Synthesis, Field-Induced Single-Ion Magnetism and Catechol Oxidase Mimicking Activity

Manisha Das,<sup>[a]</sup> Dipmalya Basak,<sup>[a]</sup> Zdeněk Trávníček,<sup>[b]</sup> Ján Vančo,<sup>[b]</sup> and Debashis Ray\*<sup>[a]</sup>

**Abstract:** Simultaneous incorporation of both Co<sup>II</sup> and Co<sup>III</sup> ions within a new thioether S-bearing phenol-based ligand system, H<sub>3</sub>L (2,6-bis-[(2-(2-hydroxyethylthio)ethylimino)methyl]-4-methylphenol) formed [Co<sub>5</sub>] aggregates [Co<sup>II</sup>Co<sup>III</sup><sub>4</sub>L<sub>2</sub>( $\mu$ -OH)<sub>2</sub>( $\mu_{1,3}$ -O<sub>2</sub>CCH<sub>3</sub>)<sub>2</sub>](ClO<sub>4</sub>)<sub>4</sub>·H<sub>2</sub>O (1) and [Co<sup>II</sup>Co<sup>III</sup><sub>4</sub>L<sub>2</sub>( $\mu$ -OH)<sub>2</sub>( $\mu_{1,3}$ -O<sub>2</sub>CC<sub>2</sub>H<sub>5</sub>)<sub>2</sub>](ClO<sub>4</sub>)<sub>4</sub>·H<sub>2</sub>O (2). The magnetic studies revealed axial zero-field splitting (ZFS) parameter,  $D/hc = -23.6$  and  $-24.3$  cm<sup>-1</sup>, and  $E/D = 0.03$  and  $0.00$ , respectively for 1 and 2. Dynamic magnetic data confirmed the complexes as SIMs with  $U_{\text{eff}}/k_B = 30$  K (1) and  $33$  K (2), and  $\tau_0 = 9.1 \times 10^{-8}$  s (1), and  $4.3 \times 10^{-8}$  s (2). The larger atomic radius of S compared

to N gave rise to less variation in the distortion of tetrahedral geometry around central Co<sup>II</sup> centers, thus affecting the  $D$  and  $U_{\text{eff}}/k_B$  values. Theoretical studies also support the experimental findings and reveal the origin of the anisotropy parameters. In solutions, both 1 and 2 which produce {Co<sup>III</sup><sub>2</sub>( $\mu$ -L)} units, display solvent-dependent catechol oxidation behavior toward 3,5-di-*tert*-butylcatechol in air. The presence of an adjacent Co<sup>III</sup> ion tends to assist the electron transfer from the substrate to the metal ion center, enhancing the catalytic oxidation rate.

## Introduction

Novel coordination aggregates of *3d* metal ions can be achieved by suitable modulation of the bridging assistance of judiciously chosen ancillary ligands.<sup>[1]</sup> In solution these ancillary ligands can often result in coordination induced aggregation of preformed fragments of selected metal ions and ligands. Playing with these ligands, either in situ generated or added from outside, in the domain of synthesis teaches us about their potential for multinuclear coordination aggregates as obtained by the competitive occupancy of available or vacant coordination sites by the primary ligand system and supporting ancillary groups. Judicious selection of primary ligand and ancillary bridges were vital to bring about the self-condensation of fragments to give rise to exciting structures.<sup>[2]</sup> In this regard phenol-based Schiff bases showed promise to extend immediate coordination to two metal ions to generate fragments suitable for aggregation. Molecular aggregates based on *3d* ions are strongly related to a variety of research fields, including bioinorganic chemistry, catalysis, structures and magnetism. Self-assembling of ligand bound fragments can result in visual-

ly pleasing shapes and structures of the compounds which can be interesting in the areas of molecular magnetism and magneto-caloric materials.<sup>[3-6]</sup>

Room-temperature synthesis, characterization and crystallization of *3d* metal ion aggregates have received considerable attention in recent years. Many of these aggregates often possess a large ground-state spin ( $S$ ) and sizeable magnetic anisotropy ( $D$ ) giving rise to sizeable barrier for reversal of magnetization,  $U_{\text{eff}}$ . Within these multimetallic aggregates either all the centers are paramagnetic or in the middle of several diamagnetic centers one or more of them could be paramagnetic. The SMM behavior under the second category having a single paramagnetic metal ion often depends on unusual coordination geometry generating a magnetically anisotropic ground state. Thus interesting types of molecular magnet can be conceived on a single paramagnetic ion, known as single-ion magnets (SIMs) and have shown promise in recent years when the choice for the *3d* ion is Co<sup>II</sup>.<sup>[7,8]</sup> Most recent advancement in the field of multinuclear Co<sup>II</sup>-based aggregates is due to the fact that they display slow magnetic relaxation at low temperature. Co<sup>II</sup>-SMMs can demonstrate much larger magnetic anisotropy and higher blocking temperatures than SMMs based on ions where the zero-field splitting originates from a second order spin-orbit coupling.<sup>[9]</sup> It is known that low-coordinate, high-spin Fe<sup>II</sup> and Co<sup>II</sup> complexes can record large and negative  $D$  values for this purpose. We have recently reported a polynuclear cobalt complex containing a single Co<sup>II</sup> ion in distorted tetrahedral geometry surrounded by diamagnetic Co<sup>III</sup> centers showing SIM behavior.<sup>[10]</sup> The trapping of Co<sup>II</sup> within a constrained environment of the surrounding Co<sup>III</sup> ions resulted in a unique distortion of the geometry from regular tetrahedra around the Co<sup>II</sup> leading to more negative  $D$  value.

[a] M. Das, D. Basak, Prof. Dr. D. Ray  
Department of Chemistry  
Indian Institute of Technology  
Kharagpur 721 302 (India)  
E-mail: dray@chem.iitkgp.ac.in

[b] Prof. Dr. Z. Trávníček, Dr. J. Vančo  
Division of Biologically Active Complexes and Molecular Magnets  
Faculty of Science  
Palacký University  
Šlechtitelů 27, 783 71 Olomouc (Czech Republic)

 Supporting information and the ORCID identification number(s) for the author(s) of this article can be found under:  
<https://doi.org/10.1002/asia.201901109>

The phenol bearing ligand ( $H_nL$ ) family with side arms on both the adjacent sides is known to provide  $\{M_2L\}^{n+}$  ( $M=3d$  metal ions) fragments having potential for self-aggregation in presence of  $HO^-/RO^-$  and  $RCO_2^-$  ions.<sup>[2]</sup> When  $M=Co$ , we have shown that aggregation of preformed  $\{Co_2L\}^{n+}$  fragments around  $CO_3^{2-}$  groups lead to a  $[Co_5]$  wheel type structure.<sup>[1]</sup> In solutions such fragments assemble together to provide the final product and these reactive species can show interesting solution properties which aid in their solution characterization. In the native state catechol oxidase (CO) catalyze the oxidation of *ortho*-diphenols by utilizing the electron transfer properties of copper ions.<sup>[11]</sup> This oxygen-utilizing enzyme controls the reactions involving  $O_2$  by modulating the reactivity of ligand-bound metal ion fragments. Functional mimetic studies were centered on  $[Cu_2]$  complexes due to the fact that CO is a Type-III copper enzyme. Recently other metal ions like  $Mn^{II/III}$  and  $Ni^{II}$  have also been used for the synthesis of such functional mimics.<sup>[12-14]</sup> The synergism between the chosen ligand and used metal ions provides a strong influence on the affinity for substrate catechol. Dinuclear and other cobalt(II/III) complexes were less extensively explored as synthetic mimics for catechol oxidation activity.<sup>[15-18]</sup>

The nature of amine parts on the two sides of the ligand ( $H_nL$ ) backbone is important from their cooperative effects for self-aggregation and trapping of substrates while showing functional behavior. Thus systematic variation of X groups between O, N and S in  $H_2N(CH_2)_2X(CH_2)_2OH$  (Figure 1) resulted in three different ligand types of contrasting coordination potential to 3d metal ions. When  $X=O$ , the resulting ligand 2,6-bis[[(2-(2-hydroxyethoxy)ethyl)imino)methyl]-4-methylphenol showed self-aggregation reactions of preformed  $\{Co^{II}_2L\}$  fragments for  $[Co_5]$  complexes achieved from the trapping of a central  $Co^{II}$  with the help of water-derived two  $HO^-$  and six  $CH_3COO^-$  ions.<sup>[19]</sup> The ether O along with the alcoholic OH remained uncoordinated and dangling. In our previous attempt to synthesize polynuclear aggregates based on cobalt ions we had utilized the ligand 2,6-bis((2-(2-hydroxyethylamino)ethylimino)methyl)-4-methyl-phenol with  $X=N$ .<sup>[10]</sup> Reactions of the ligand with  $Co(ClO_4)_2 \cdot 6H_2O$  in the presence of externally added  $NaCOOR$  ( $R=Me, CH_2Me$ ) resulted in mixed valence pentanuclear aggregates arising from the entrapment of a central  $Co^{II}$  ion by the initially formed  $\{Co^{III}_2(\mu-L)(\mu-OH/OMe)\}$  fragments.

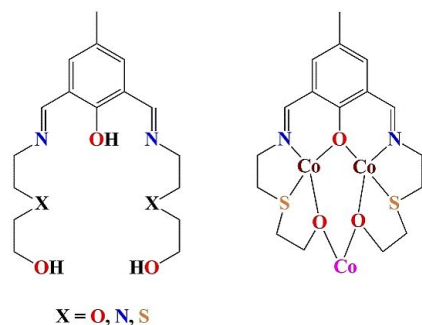
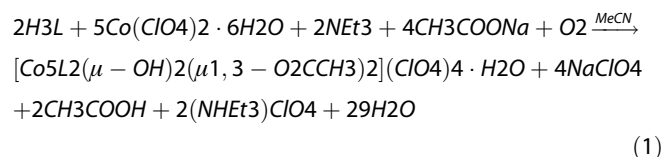


**Figure 1.** The ligand  $H_3L$  used in present work and its observed metal binding mode.

The deprotonated alcohol arm extends its coordination and bridges the ligand bound  $Co^{III}$  and the central  $Co^{II}$  trapping it in a tetrahedral environment. In our present investigation we have extended our idea by introducing a bigger thioether S donor hence synthesising the ligand (2,6-bis-[[2-(2-hydroxyethylthio)ethylimino)methyl]-4-methylphenol) ( $H_3L$  when  $X=S$ ; Figure 1 left). We have investigated the reactivity of  $H_3L$  (Figure 1 right) with  $Co(ClO_4)_2 \cdot 6H_2O$  in the presence of two different carboxylate salts ( $RCO_2^-$ ,  $R=Me, CH_2Me$ ) and present the synthesis of mixed-valence-mixed-geometry  $[Co_5]$  aggregates  $[Co^{II}Co^{III}_4L_2(\mu-OH)_2(\mu_{1,3}-O_2CCH_3)_2](ClO_4)_4 \cdot H_2O$  (1) and  $[Co^{II}Co^{III}_4L_2(\mu-OH)_2(\mu_{1,3}-O_2CC_2H_5)_2](ClO_4)_4 \cdot H_2O$  (2) having similar molecular structures with  $X=N$ . It is most likely that S being larger in size as compared to N will introduce more flexibility in the alcohol arm in turn affecting the amount of distortion in the tetrahedral geometry around the trapped  $Co^{II}$  ion and hence the magnitude of  $D$ . The synthesis, growth of crystals, X-ray structure determinations, magnetic properties and catechol oxidation activity of these complexes are described and discoursed. Recently we have shown that use of  $H_3L$  resulted only  $\{Cu_2L(OH)\}^{2+}$  based complexes without showing any kind of self-aggregation around nucleating anions or metal ions from the reaction medium.<sup>[20]</sup> Catalytic catechol oxidation studies in different solvent medium showed the influence of the ligand alcohol arm on the mechanism of substrate oxidation under aerobic conditions. In this work we have investigated the solvent dependent catalytic potency of  $\{Co^{III}_2L\}$  fragments generated in solution towards oxidation of 3,5-DTBC $H_2$ .

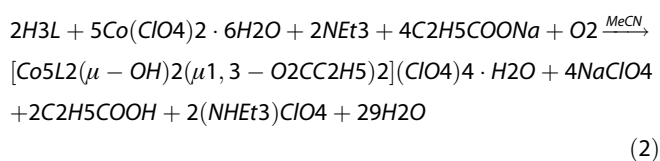
## Results and Discussion

**Single Step Aggregation Reaction.** Phenol-based and thioether sulfur side arm bearing ligand has been developed from the synthesis of 2-(2-aminoethylthio)ethanol. This amine-alcohol having thioether sulfur donor at the center was prepared from the reaction of 2-mercaptoethanol in 30% aqueous NaOH solution and 2-chloroethylamine hydrochloride in aqueous medium. The ligand 2,6-bis-[[2-(2-hydroxyethylthio)ethylimino)methyl]-4-methylphenol ( $H_3L$ ) was acquired from the reaction of 2,6-diformyl-4-methylphenol and 2-(2-aminoethylthio)ethanol in refluxing MeOH medium. In MeCN medium reaction of  $H_3L$ ,  $Co(ClO_4)_2 \cdot 6H_2O$ ,  $NEt_3$  and  $CH_3COONa$  in 1:2.5:1:2 ratio under stirring and refluxing condition resulted in a deep brown solution from which brown block shaped crystals of **1** were obtained after 18 days in 67% yield [Eq. (1)]. Different sequence of addition of reactants and changes in molar ratios of the components failed to give any other type of complex



In a similar fashion, use of  $C_2H_5COONa$  in MeCN in lieu of  $CH_3COONa$  and same molar ratio gave a brown solution after 45 min of room temperature stirring followed by 1 h reflux.

Brown crystals of **2** were obtained from this solution after 20 days (0.478 g, 59% yield) [Eq. (2)].



Elemental analysis and single crystal X-ray determination provided the composition of **1** and **2** as  $[\text{Co}_5\text{L}_2(\mu\text{-OH})_2(\mu_{1,3}\text{-O}_2\text{CCH}_3)_2](\text{ClO}_4)_4 \cdot \text{H}_2\text{O}$  and  $[\text{Co}_5\text{L}_2(\mu\text{-OH})_2(\mu_{1,3}\text{-O}_2\text{CC}_2\text{H}_5)_2](\text{ClO}_4)_4 \cdot \text{H}_2\text{O}$ . Thus in solution, two  $\{\text{Co}^{\text{III}}_2\text{L}(\text{OH})\}^{2+}$  units were responsible to give a tetrahedral  $\text{O}_4$  coordination pocket to trap the fifth metal ion in the aggregate as a single paramagnetic  $\text{Co}^{\text{II}}$  center (Scheme 1).

**FT-IR Characterization of Powdered Samples.** Compounds **1** and **2** were used as KBr pellets for immediate identification following synthesis. The appearance of broad peaks at  $3412$  and  $3421\text{ cm}^{-1}$  in the spectra confirmed the presence of hydroxido group and water molecule in the crystal lattices. The coordination from imine functions of the ligand was recognized from the  $\nu_{\text{C=N}}$  stretching frequency at  $1648$  and  $1647\text{ cm}^{-1}$  for **1** and **2** respectively. The asymmetric ( $\nu_{\text{as}(\text{COO})}$ ) and symmetric ( $\nu_{\text{s}(\text{COO})}$ ) stretching vibrations for bridging acetate groups in **1** appeared at  $1576$  and  $1430\text{ cm}^{-1}$  (Figure S1 in the Supporting Information). In case of **2** the presence of propionate bridges were detected at  $1577$  and  $1459\text{ cm}^{-1}$ . The  $\Delta\nu$  values ( $146\text{ cm}^{-1}$  for **1** and  $118\text{ cm}^{-1}$  for **2**) confirmed the carboxylate bridging modes as  $\mu_{1,3}$  type in both the cases.<sup>[21]</sup> The presence of four perchlorate (in  $T_d$  symmetry) ions were also detected uniformly at  $1090$ ,  $626$  and  $625\text{ cm}^{-1}$  due to the  $\nu_3(T_2)$  ( $\nu_{\text{ClO}}$ ) and  $\nu_4(T_2)$  ( $\delta_{\text{d}(\text{ClO})}$ ) stretching modes, respectively.<sup>[22]</sup>

## Crystal Structures Descriptions

$[\text{Co}^{\text{III}}_4\text{L}_2(\mu\text{-OH})_2(\mu_{1,3}\text{-O}_2\text{CCH}_3)_2](\text{ClO}_4)_4 \cdot \text{H}_2\text{O}$  (**1**). The molecular structure of the tetracationic part of **1** is shown in Figure 2, and important bond distances and angles are provided in Table S1 in Supporting Information. Complex **1** crystallizes in orthorhombic  $Fdd2$  space group with  $Z=16$  and the asymmetric unit consists of one pentanuclear fragment  $[\text{Co}_5\text{L}_2(\mu\text{-OH})_2(\mu_{1,3}\text{-O}_2\text{CCH}_3)_2]^{4+}$ , four perchlorate anions and a lattice water molecule.

A remarkable mixed-valence-mixed-geometry pentanuclear aggregate has been identified from the coordination support of imine-thioether-alcohol arm and imine-phenolate backbone from two  $\text{L}^{3-}$  units. The  $[\text{Co}_5]$  aggregate consists of two  $\text{L}^{3-}$ , each of them delivering two neighboring ONSO pockets to bind two smaller  $\text{Co}^{\text{III}}$  ions. Trapping of in situ generated  $\text{HO}^-$  ions by initially formed  $\{\text{Co}^{\text{III}}_2(\mu\text{-L})\}$  units provided  $\{\text{Co}^{\text{III}}_2\text{L}(\text{OH})\}$  fragments. In the following step the growth of **1** may be assumed to happen by the aggregation of two  $\{\text{Co}_2(\mu\text{-L})(\mu\text{-OH})(\mu\text{-O}_2\text{CCH}_3)\}$  units, obtained from the capping of carboxyl-

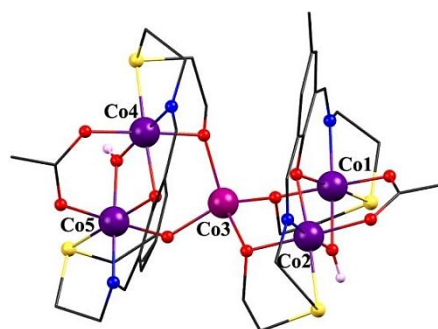
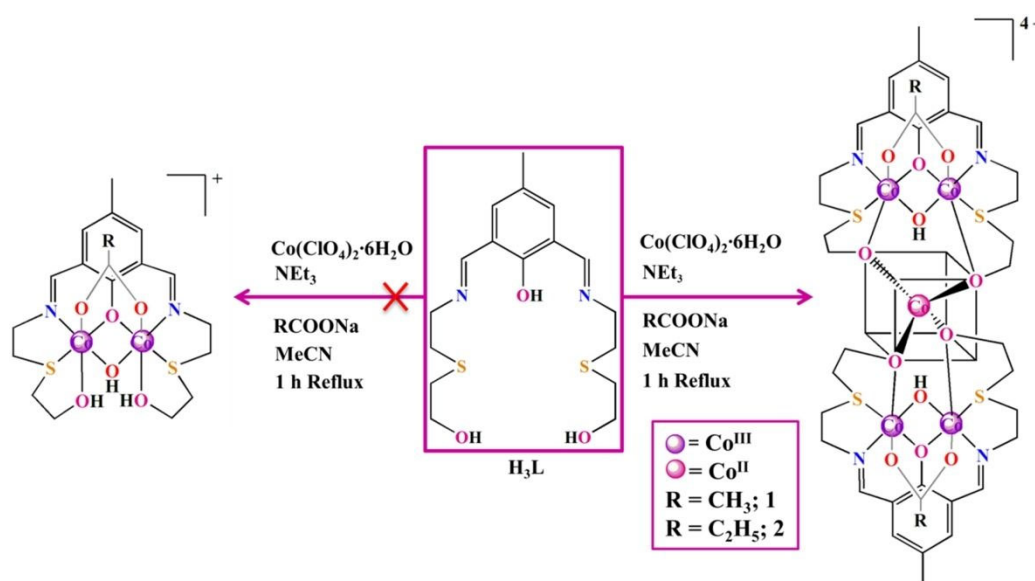


**Figure 2.** POV-ray view of the cationic part **1** with partial atom numbering Scheme. H atoms are omitted for clarity. Color code: C, black; N, blue; O, red; S, yellow;  $\text{Co}^{\text{III}}$ , violet;  $\text{Co}^{\text{II}}$ , purple.



**Scheme 1.** Synthetic routes for **1** and **2**.

ate anions, around the fifth and central  $\text{Co}^{\text{II}}$  ion in *pseudo-tetrahedral* geometry in the final structure. Simultaneous bridging by ligand phenoxido and ancillary hydroxido and carboxylato groups maintained the  $\text{Co}\cdots\text{Co}$  separation within 2.779–2.802 Å range (Table S3 in Supporting Information). The *facial* folding of the imine-thioether-alcohol (NSO) arms of  $\text{L}^{3-}$  was vital for the *tetrahedral* disposition of four oxygen atoms around the central  $\text{Co}^{\text{II}}$  center. The four  $\text{Co}^{\text{III}}$  centers (Co1, Co2, Co3 and Co4) stay in distorted *octahedral*  $\text{NSO}_4$  coordination geometry (Figure 3).

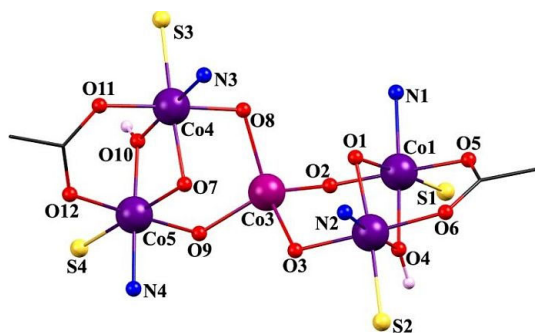


**Figure 3.** Core view of **1** showing two types of cobalt centers. Color code: C, black; N, blue; O, red; S, yellow;  $\text{Co}^{\text{III}}$ , violet,  $\text{Co}^{\text{II}}$ , purple.

The Co–N distances for imine coordination around the  $\text{Co}^{\text{III}}$  centers are shorter at 1.894(10)–1.935(11) Å compared to Co–S distances for thioether coordination involving bigger sulfur atoms in 2.198(4)–2.206(3) Å range. The phenoxido bridges from the  $\text{L}^{3-}$  units regulate the  $\text{Co}^{\text{III}}\text{-O}_{\text{ph}}\text{-Co}^{\text{III}}$  angles to 92.3(3)–93.2(3)°, while the exogenous  $\text{HO}^-$  bridges were responsible for Co– $\text{O}_{\text{hy}}\text{-Co}$  angles in 94.3(4)–95.3(4)° range. The terminal alkoxido groups from the NSO arms asymmetrically bridge the *octahedral*  $\text{Co}^{\text{III}}$  and *tetrahedral*  $\text{Co}^{\text{II}}$  centers during aggregation. As expected the  $\text{Co}^{\text{III}}\text{-O}$  separations were shorter (1.880(8)–1.931(8) Å range) for the four types of oxygen donors compared to that in case of the tetrahedral  $\text{Co}^{\text{II}}$  centers (Co–O separations in 1.991(8)–2.031(8) Å range). For the *facial* folding of the NSO arms the C–S–C angles remain within 102.3(9)–105.5(8)° range compared to the larger C–N–C angles in 113.0(6)–117.3(2)° range reported for analogous complex in our previous work<sup>[10]</sup> signifying greater amount of folding in presence of S. The O–Co–O angles around the central *tetrahedral*  $\text{Co}^{\text{II}}$  ion span from 100.9(3)–133.4(3)°. The Houser's geometry index  $\tau_4$  ( $\tau_4 = [360^\circ - (\alpha + \beta)]/141^\circ$ ;  $\alpha$  and  $\beta$  being the two largest angles) for the central  $\text{Co}^{\text{II}}$  ion is 0.83 indicating at slightly distortion of the  $T_d$  geometry.<sup>[23]</sup> For a perfect *tetrahedral* environment  $\tau_4$  value is 1.00 while for an ideal *square planar* geometry the value is 0.00.

The assignment of +3 and +2 oxidation states to *octahedral* and *tetrahedral* cobalt ion centers were evident from the bond distances and were further confirmed by BVS analysis (Table S2 in Supporting Information).<sup>[24,25]</sup>

$[\text{Co}^{\text{III}}\text{Co}^{\text{II}}_4\text{L}_2(\mu\text{-OH})_2(\mu_{1,3}\text{-O}_2\text{CC}_2\text{H}_5)_2](\text{ClO}_4)_4 \cdot \text{H}_2\text{O}$  (**2**). The tetracationic part of **2** within the molecular structure is depicted in Figure 4, and important bond distances and angles are given

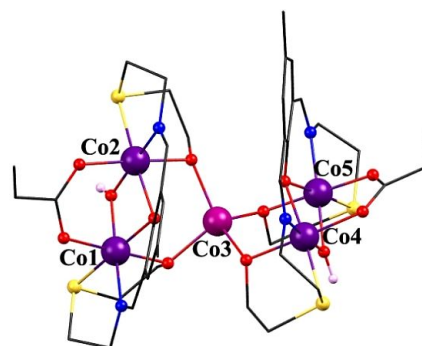


**Figure 4.** POV-ray view of the cationic part of **2** with partial atom numbering Scheme. H atoms are omitted for clarity. Color code: C, black; N, blue; O, red; S, yellow;  $\text{Co}^{\text{III}}$ , violet,  $\text{Co}^{\text{II}}$ , purple.

in Table S2 in Supporting Information. Complex **2** crystallize in monoclinic  $P2_1/c$  space group with  $Z=4$ . The asymmetric unit of **2** consists of one  $[\text{Co}_5\text{L}_2(\mu\text{-OH})_2(\mu_{1,3}\text{-O}_2\text{CC}_2\text{H}_5)_2]^{4+}$  part, four perchlorate anions and one lattice water molecule. Here two  $\{\text{Co}^{\text{III}}_2(\mu\text{-L})\}$  units bridged by  $\text{HO}^-$  and  $\text{C}_2\text{H}_5\text{COO}^-$  groups, assemble around the tetrahedral  $\text{Co}^{\text{II}}$  ion to provide **2**. The structure and all other metric parameters are similar to those for complex **1** (Figure 5). The triply-bridged situation in  $\{\text{Co}_2(\mu\text{-L})\}$  units in the final structure ensued a  $\text{Co}\cdots\text{Co}$  separations of 2.785 Å. The distorted *octahedral*  $\text{NSO}_4$  coordination geometry around  $\text{Co}^{\text{III}}$  centers are formed from coordination of four types of oxygen atoms along with imine nitrogen and thioether sulfur atoms. The Co–N and Co–S separations were in the ranges of 1.889(7)–1.908(7) and 2.194(2)–2.203(3) Å, respectively. The  $\text{Co}^{\text{III}}\text{-O}$  bond lengths from the bridging phenoxido, hydroxido, propanoato groups within the  $\{\text{Co}_2(\mu\text{-L})(\mu\text{-OH})(\mu\text{-O}_2\text{CC}_2\text{H}_5)\}$  fragments were in 1.879(5)–1.937(5) Å range. Within the flattened *tetrahedral* cavity (Houser's  $\tau_4=0.82$ ) the  $\text{Co}^{\text{II}}\text{-O}$  bonds were longer at 1.989(6)–2.043(5) Å. The O–Co–O angles around this ion span from 97.2(19) to 134.3(2)°. The C–S–C angles were found within 102.0(5)–104.4(5)° range which is similar to that in **1**. In comparison, the C–N–C angles for the analogous compound previously reported by us fall in 109.3(2)–114.5(3)° range which deviates considerably compared to that recorded for  $\text{CH}_3\text{CO}_2^-$  bridges (113.0(6)–117.3(2)°).<sup>[10]</sup> The very similar  $\tau_4$  value compared to **1** confirmed almost negligible effect on the compression of the tetrahedral geometry around central  $\text{Co}^{\text{II}}$

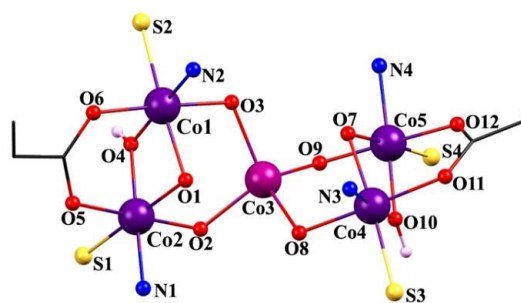


**Figure 5.** Core view of **2**. Color code: C, black; N, blue; O, red; S, yellow;  $\text{Co}^{\text{III}}$ , violet,  $\text{Co}^{\text{II}}$ , purple.

due to bridging of the ligand bound  $\text{Co}^{\text{III}}$  centers by the  $\text{C}_2\text{H}_5\text{CO}_2^-$  groups in place of  $\text{CH}_3\text{CO}_2^-$ . In our previous investigation the variation in  $\tau_4$  values were greater for analogous compounds.<sup>[10]</sup> This can be substantiated from the variation of C-X-C (X=N, S) bond angles with the larger size of S compensating for any structural strains introduced by the change in bridging carboxylate. BVS analysis confirmed a +3 oxidation state for the *octahedral* cobalt ions and +2 oxidation state for *tetrahedral* cobalt ions (Table S2 in Supporting Information).

**Magnetic properties.** Investigation of the magnetic features of complexes **1** and **2** proceeded firstly using a PPMS device on which the temperature (1.9–300 K) and field (0–9 T) dependent magnetic data were obtained and they are shown in Figure 6. The magnetic properties of the complexes are primarily due to the presence of central *tetrahedral*  $\text{Co}^{\text{II}}$  ion since *octahedral* LS- $\text{Co}^{\text{III}}$  ions are diamagnetic. The value of effective magnetic moment ( $\mu_{\text{eff}}$ ) of complex **1** at 300 K is  $4.5 \mu_{\text{B}}$ , higher than the spin-only value of  $3.9 \mu_{\text{B}}$  for  $S=3/2$ ,  $g=2.0$ . Thereafter

upon cooling the  $\mu_{\text{eff}}$  value decrease gradually upto *ca* 50 K and then, it drops sharply to a minimum at 1.9 K, where it adopts the value of  $3.3 \mu_{\text{B}}$ . In the case of complex **2**, the  $\mu_{\text{eff}}$  value at 300 K is  $5.4 \mu_{\text{B}}$ , which is again much higher than the calculated value for isotropic  $S=3/2$  spin. It decreases gradually upon cooling up to *ca* 50 K and then, it declines sharply to a minimum at 1.9 K reaching the value of  $3.9 \mu_{\text{B}}$ . The high  $\mu_{\text{eff}}$  values at 300 K indicates considerable contribution of a spin-orbit coupling to the ground state in both the complexes. Isothermal magnetization experiments (Figure 6) for **1** and **2** in the applied field range of  $B=0-9$  T at different constant temperatures  $T=2, 5$  and 10 K reveal that the magnetization does not show saturation suggesting the presence of magnetic anisotropy. To extract the parameters affected by magnetic anisotropy arising from crystal field effects ( $g, D$ ), both the susceptibility and magnetization data were fitted simultaneously. The best fit parameters were calculated using the PHI program package<sup>[26]</sup> for  $S=3/2$  and they are as follows:  $g_{\text{iso}}=2.29$ ,  $D=$

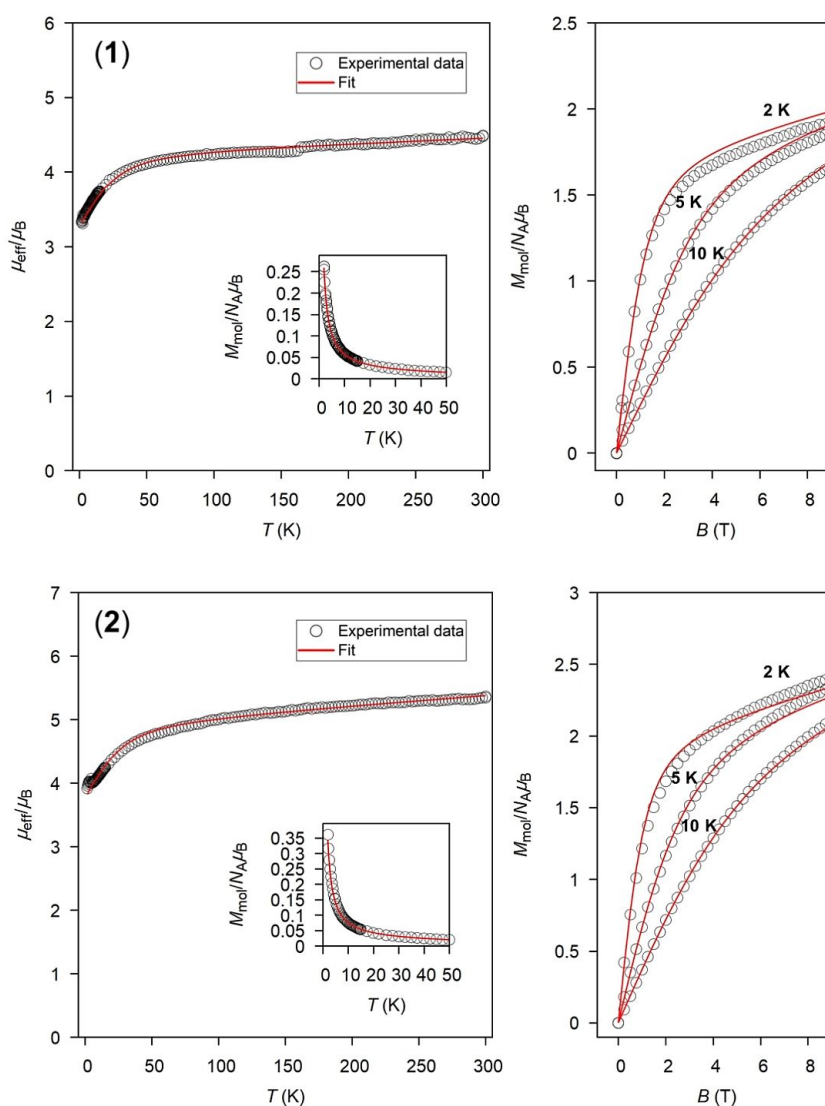


**Figure 6.** Temperature dependence of the effective magnetic moment (inset: temperature dependence of the molar magnetic susceptibility) for complexes **1** and **2** (Left). The isothermal magnetizations measured in the range of  $B=0-9$  T and at  $T=2, 5$  and 10 K (Right).

$-23.6 \text{ cm}^{-1}$ ,  $E/D=0.03$ ,  $zJ/hc=0 \text{ cm}^{-1}$ ,  $\chi_{\text{TIP}}=10.3 \times 10^{-9} \text{ cm}^3 \cdot \text{mol}^{-1}$  for **1** and  $g_{\text{iso}}=2.32$ ,  $D=-24.3 \text{ cm}^{-1}$ ,  $E/D=0.00$ ,  $zJ/hc=0.05 \text{ cm}^{-1}$ ,  $\chi_{\text{TIP}}=26.9 \times 10^{-9} \text{ cm}^3 \cdot \text{mol}^{-1}$  for **2**. The presence of temperature-independent paramagnetism (TIP) term accounts for the four surrounding  $\text{Co}^{\text{III}}$  ions. The observed  $D$  values for **1** and **2** are relatively close compared to those ( $-31.31 \text{ cm}^{-1}$  and  $-21.88 \text{ cm}^{-1}$ ) obtained in our previous investigations with complexes having similar molecular structures.<sup>[10]</sup> Incorporation of thioether S donors at the side arms in place of N donors used in our previous work, provided new ligand system  $\text{H}_3\text{L}$  utilized in the present work. Due to the larger atomic size of S, it is able to accommodate more strain in geometry around itself compared to N thus in turn reducing the difference in distortion of the central  $\text{Co}^{\text{II}}$  ion from ideal tetrahedral geometry. This is evident from the similar  $\tau_4$  values (0.83 and 0.82) calculated for **1** and **2**. The greater difference in the values of the  $D$  term observed for the complexes used in our earlier study arose from the fact that one of them showed greater distortion of the tetrahedral geometry around the central  $\text{Co}^{\text{II}}$  compared to the other.

With the aim to describe the geometry around the cobalt centres more deeply, the analysis of coordination polyhedra was performed using the SHAPE 2.1 software.<sup>[27]</sup> Based on the single-crystal X-ray data, the hexa-coordinated cobalt(III) centres (i.e. Co1, Co2, Co4, and Co5) and tetra-coordinated cobalt(II) centre (Co3) were analysed in the structures of com-

plexes **1** and **2**. The SHAPE analyses revealed that the cobalt(III) centres in both the complexes, labelled as Co1, Co2, Co4 and Co5, show nearly octahedral geometry (with the values of the deviations from the minimal distortion paths from the ideal octahedral coordination polyhedron in the range from 0.354 to 0.468), while the geometry in the vicinity of the cobalt(II) atom, labelled as Co3, can be described as slightly distorted tetrahedral (with the values of 1.510 for complex **1**, and 1.777 for complex **2**, of the deviations from the minimal distortion paths from the ideal tetrahedron). The complete results can be found in Supporting Information (see Tables S4 and S5).

Due to the presence of large anisotropy suggested by the negative  $D$  values for **1** and **2**, the dynamic magnetic data for the complexes were acquired and thus, alternate current (AC) susceptibility measurements were performed in zero and non-zero static magnetic field. Whilst in the zero static magnetic field no out-of-phase susceptibility ( $\chi''$ ) signal was observed, the measurement at an external dc field  $B_{\text{dc}}=0.1 \text{ T}$  revealed a frequency-dependent out-of-phase signal in **1** and **2**. For **1**, the single maxima was observed in the frequency range 130–1490 Hz and in the temperature range of 2.15–4.18 K while for **2**, the same appeared in the range 240–1490 Hz and 3.47–4.30 K (Figures 7 and 8). Since the peak maxima are frequency dependent, both the complexes can be considered as field-induced single-ion magnets (SIMs). A Debye model for single relaxation time was utilized to fit the data in both the cases. For

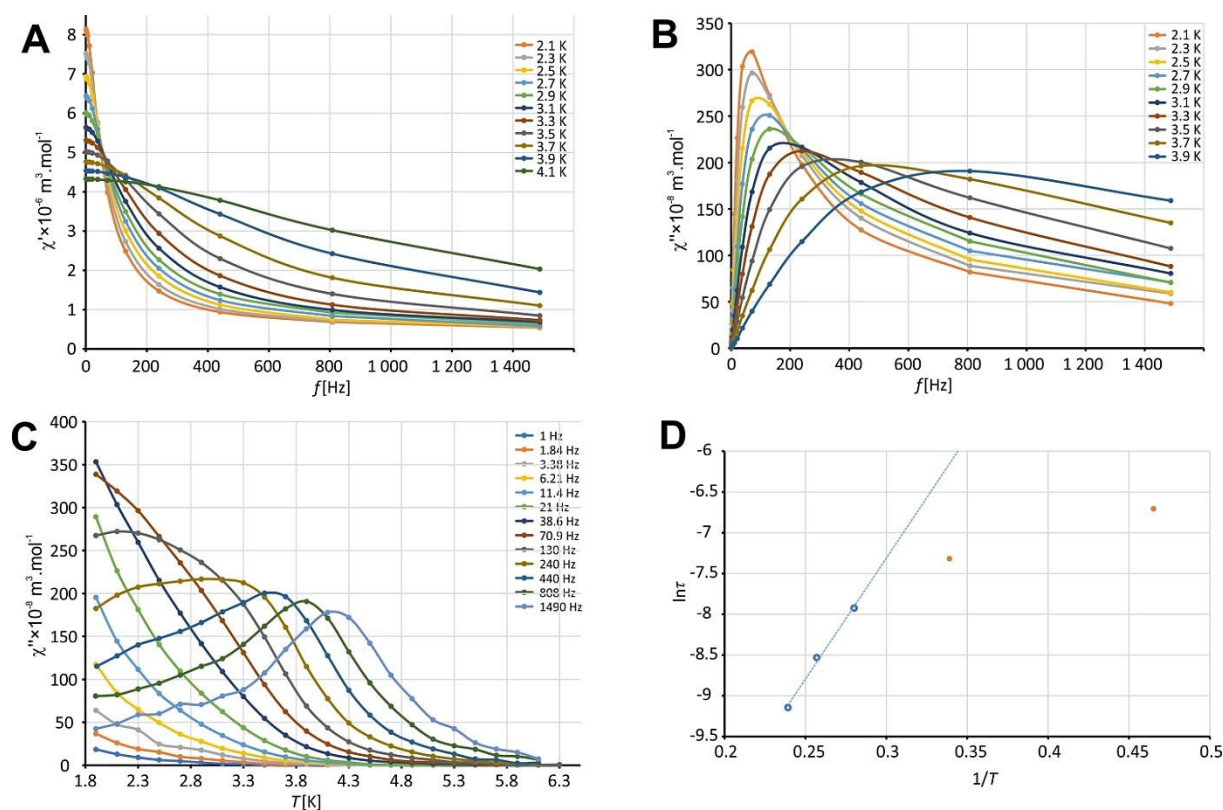


**Figure 7.** The frequency dependence of (A) in-phase  $\chi'$  and (B) out-of-phase  $\chi''$  molar susceptibilities for **1** at an applied external magnetic field  $B=0.1 \text{ T}$ . (C) The temperature dependence of the out-of-phase  $\chi''$  molar susceptibility for **1** at an applied external magnetic field  $B=0.1 \text{ T}$ . (D) The Arrhenius-like plot revealing the association with the Orbach relaxation process dominant above the temperature of 3.57 K and other type of processes contributing to the relaxation proceeding below this temperature (represented by the orange points).

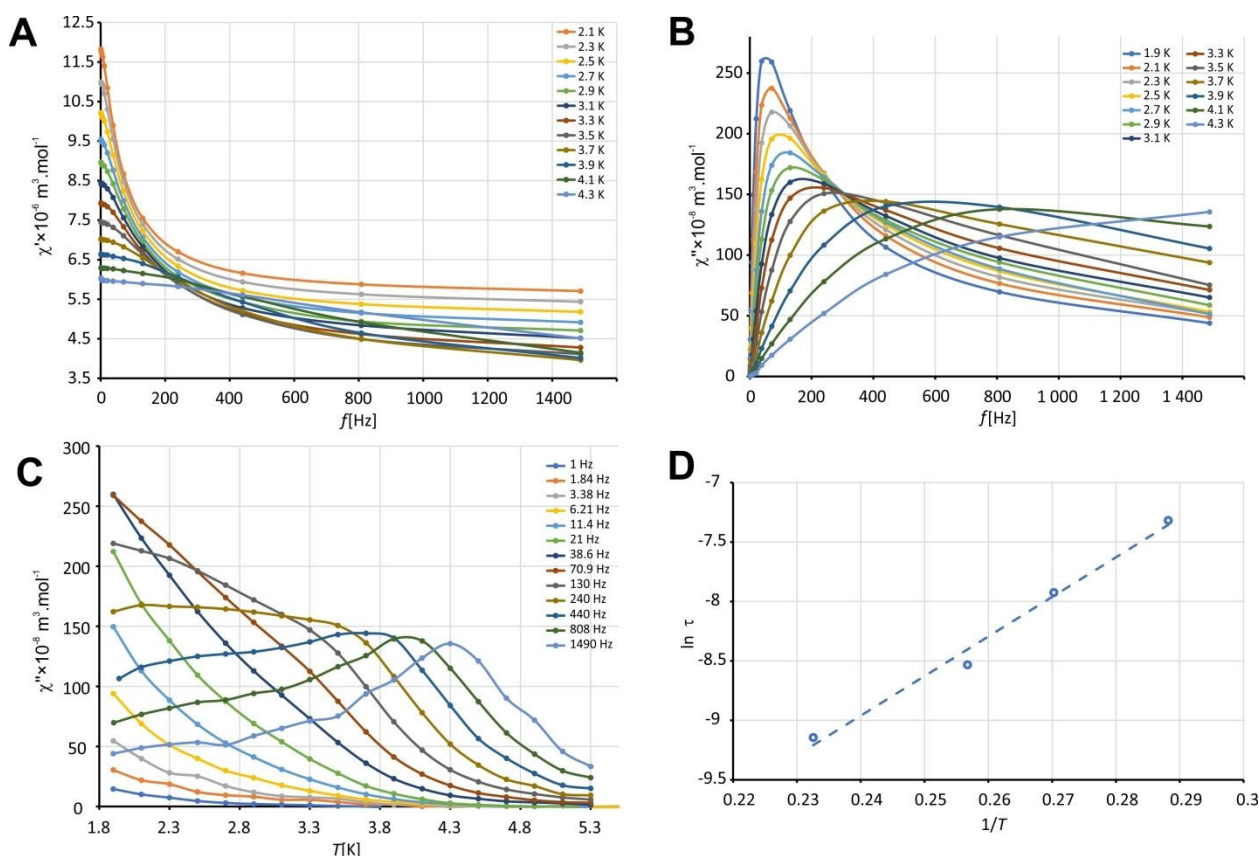


**Figure 8.** The frequency dependence of (A) in-phase  $\chi'$  and (B) out-of-phase  $\chi''$  molar susceptibilities for **2** at an applied external magnetic field  $B=0.1$  T. (C) The temperature dependence of the out-of-phase  $\chi''$  molar susceptibility for **2** at an applied external magnetic field  $B=0.1$  T. (D) The Arrhenius-like plot revealing the association with the Orbach relaxation process above the temperature of 3.45 K.

**1**, fitting of the  $\ln \tau$  vs.  $1/T$  data utilizing the Arrhenius expression reveal the dominance of Orbach relaxation process at higher temperatures ( $>3.57$  K) while at lower temperatures other types of processes like Raman relaxation process also contribute to the magnetization relaxation (Figure 7D). A similar observation was made in case of **2** and both data were fitted in the higher temperature region to obtain the values of relaxation time ( $\tau_0$ ) and spin reversal barrier ( $U_{\text{eff}}/k_B$ ). The parameters obtained are as follows:  $\tau_0=9.1 \times 10^{-8}$  s (**1**), and  $4.3 \times 10^{-8}$  s (**2**), and  $U_{\text{eff}}/k_B=30$  K (**1**) and 33 K (**2**). The values of  $U_{\text{eff}}/k_B$  are very similar to that obtained for a simple complex  $[\text{Co}(\text{PPh}_3)_2\text{Br}_2]$  with  $U_{\text{eff}}/k_B=37$  K.<sup>[28]</sup> The  $U_{\text{eff}}/k_B$  values for **1** and **2** are close to each other as expected from their very similar  $D$  values. Thus the amount of distortion in geometry of the central tetrahedral  $\text{Co}^{\text{II}}$  can be varied through change in donor atom of the ligand backbone which in turn affects the anisotropy parameter  $D$  and spin reversal barrier ( $U_{\text{eff}}/k_B$ ). In our previous investigation we had shown that the magnitude of single-ion  $D$  term for pseudo-mononuclear  $\text{Co}^{\text{II}}$  units can be altered by trapping them within a predefined diamagnetic environment.<sup>[10]</sup> In the present study we have been able to demonstrate that the use of donor atoms with larger atomic radii like S in the same ligand backbone instead of N gives rise to lesser variation in  $D$  and  $U_{\text{eff}}/k_B$  values and *vice-versa*. Thus an effective method for altering the various anisotropy parameters as-

sociated with single ion  $\text{Co}^{\text{II}}$  can be formulated from these collective findings.

To further corroborate the results obtained from experimental measurements and to better understand the origin of the various anisotropy parameters, we have performed CASSCF calculations employing NEVPT2 correction on the X-ray crystal structures of **1** and **2**. The zero-field splitting parameters were determined using the Hamiltonian [Eq. (3)]<sup>[29–32]</sup>

$$\hat{H}_{\text{ZFS}} = D[\hat{S}_z^2 - S(S+1)/3] + E(\hat{S}_x^2 - \hat{S}_y^2) \quad (3)$$

where  $D$  is the axial zero-field splitting (ZFS) parameter,  $E$  is the rhombic ZFS parameter, and  $S$ ,  $S_x$ ,  $S_y$  and  $S_z$  are the total spin and its  $x$ ,  $y$ , and  $z$  components, respectively. The three diagonal components of the  $D$  tensor are  $D_{ZZ}$ ,  $D_{YY}$  and  $D_{XX}$  and  $D$  is related to  $D_{ZZ}$  as  $D=3/2 D_{ZZ}$ . Thus the overall sign of  $D$  can be obtained by analyzing the sign of  $D_{ZZ}$ . The NEVPT2 method yielded a  $D$  value of  $-20.7 \text{ cm}^{-1}$  and  $E/D$  value of 0.14 for complex **1** while for complex **2** these were found to be  $D=-24.0 \text{ cm}^{-1}$  and  $E/D=0.17$  (Table 1). The obtained values are close to those obtained experimentally. The Loewdin orbital-compositions for the d-based CASSCF orbitals for complexes **1** and **2** are shown in Tables S5 and S6 in Supporting Information. The ground state wave function shows slight mixing with excited states as shown in Tables S7 and S8 in Supporting Infor-

**Table 1.** Experimental and computed Spin Hamiltonian Parameters for Complexes 1 and 2.

Complex	Experimental			Calculated (NEVPT2)		
	$D$ [ $\text{cm}^{-1}$ ]	$E/D$	$g_{\text{iso}}$	$D$ [ $\text{cm}^{-1}$ ]	$E/D$	$g_{\text{iso}}$
1	-23.6	0.03	2.29	-20.7	0.14	2.28
2	-24.3	0.00	2.32	-24.0	0.17	2.29

mation with the major configuration possessing about 93% and 90% weightage for complexes 1 and 2 respectively. This suggests that a single electron configuration cannot explain the given ligand field state. Both the complexes are close to  $D_{2d}$  symmetry leading to less mixing at the ground state wave function as compared to our previous work. Due to less variation in the geometry around the central  $\text{Co}^{\text{II}}$  ion when comparing complex 1 with 2, both of them show similar high weightage of the major configuration. This is in contrast to our previous study where a considerable difference in the weightage of the major configuration was observed (41% and 62%). Figure 9 represents the eigenvalue plots of the d-based CASSCF orbitals for complexes 1 and 2.

The major contribution to the negative  $D$  parameter in complex 1 comes from  $\Psi_2 \rightarrow \Psi_3$  (43%) and  $\Psi_1 \rightarrow \Psi_3$  (43%) electron-

ic transitions (Table S6 in Supporting Information). For complex 2 the contribution comes from  $\Psi_1 \rightarrow \Psi_3$  (55%) and  $\Psi_2 \rightarrow \Psi_3$  (36%) transitions (Table S7 in Supporting Information). The energy gap between the  $\Psi_1$  and  $\Psi_3$  orbitals and  $\Psi_2$  and  $\Psi_3$  orbitals are very similar in both the complexes which is expected from the similar torsional angle ( $\theta$ ) in complex 1 (100 and 101°) and complex 2 (97 and 99°). Figure 10 represents the  $D$  and  $g$  anisotropy axes of complexes 1 and 2. The structural parameter which controls the  $D$  value is the O-Co-O or torsion angle<sup>[33]</sup> while the  $E/D$  value is controlled by the interplanar or dihedral angle<sup>[34]</sup> (Table 2). Both complexes 1 and 2 have very similar torsion angles which explains the closeness of the  $D$  values. In our previous study, due to greater difference in the torsion angle, the  $D$  values were also widely spaced. Thus in-

**Table 2.** Structural parameters affecting the magnitude of  $D$  and  $E/D$  in complexes 1 and 2.

Complex	Dihedral angle [ $\theta_{\text{d}}$ , deg]	Torsional angle [ $\theta_{\text{t}}$ , deg]	$D$ [ $\text{cm}^{-1}$ ]	$E/D$
1	78.05	O9-Co3-O3 = 101.43, O8-Co5-O2 = 100.94	-20.7	0.14
2	75.71	O8-Co5-O2 = 99.72, O9-Co3-O3 = 97.26	-24.0	0.17

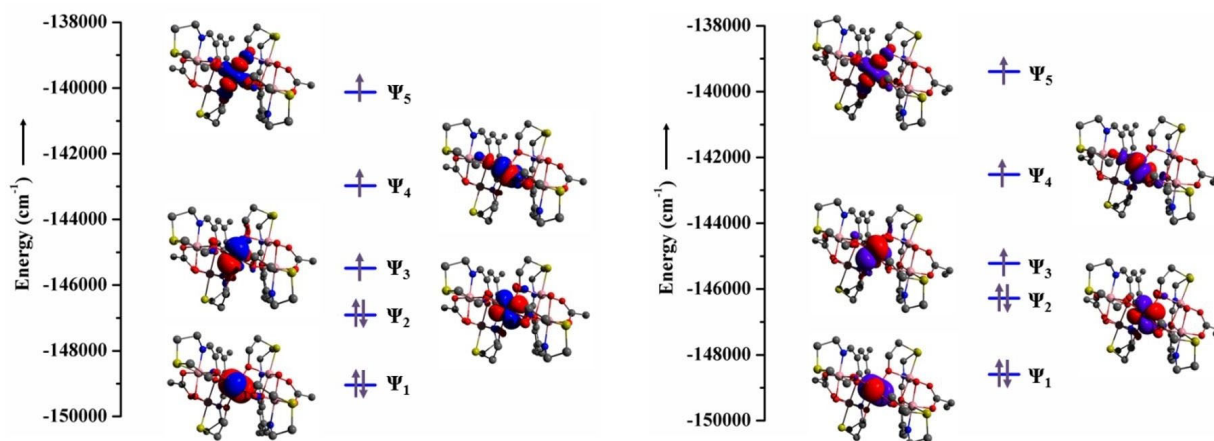


**Figure 9.** Energy levels of d-based CASSCF orbitals of complex 1 (left) and complex 2 (right).

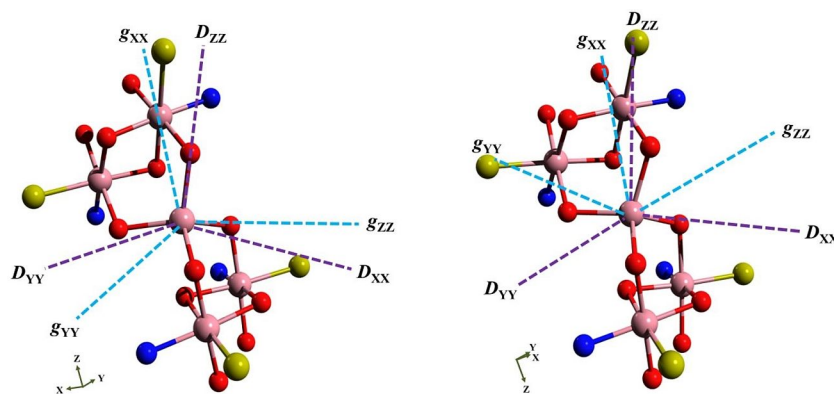


**Figure 10.**  $D$  and  $g$  anisotropy axes of complexes 1 (left) and 2 (right). Colour code: Co, pink; O, red; N, blue; S, yellow (C and H atoms are omitted for clarity).

roduction of larger donor atom S in place of N in the ligand backbone tends to relax the distortion of the  $\{CoO_4\}$  tetrahedron brought about by the constrained environment produced by the diamagnetic  $Co^{III}$  ions and effectively alters the various anisotropic parameters.

**Functional Behavior for catechol oxidation.** Variety of catechol molecules are found extensively in nature and used for several functions, including neurotransmission, pigment formation, surface adhesion, protein crosslinking and formation of beak and cuticle materials as well as microbial iron ion uptake in siderophores. Till today laboratory synthesized  $Co^{III/II}$  complexes have been comparatively less probed as synthetic imitators for catechol oxidase like functions. The motivation to model the enzyme active sites originates from the potential of the aggregating fragments to act as efficient catalyst in order to afford insight into the mechanistic pathways of the native enzymes in the line of designing man made catalysts. Further to this, in recent year opinions from clinical trials and epidemiological studies support the hypothesis that estrogen contributes to breast cancer and may be a pertinent agent. The oxidative metabolites of estrogen have been implicated in chemical carcinogenesis. Oxidation of the catechol metabolite of estrone gives o-quinones that produce reactive oxygen species (ROS) and damage DNA by adduct formation and oxidation.<sup>[35]</sup>

Herein we examined the ability of complexes **1** and **2** to produce catalytically active fragments in solution to oxidize 3,5-*tert*-butylcatechol (3,5-DTBCH<sub>2</sub>) in air to the quinone form.

Choice of this model substrate to monitor the reaction originates from the presence of tertiary butyl groups on the catechol ring thereby reducing the oxidation potential while preventing further oxidation and ring-opening reaction.<sup>[36]</sup> Two different solvent media MeOH and MeCN were used to compare the reaction rate for the formation of 3,5-DTBQ at 401 and 403 nm, respectively. Solutions of **1** and **2** ( $\approx 1 \times 10^{-5} \text{ mol L}^{-1}$ ) were treated with 100 equiv of 3,5-DTBCH<sub>2</sub> in MeOH and MeCN respectively and time dependent UV-vis spectra were recorded under aerobic conditions up to 50 min at 5 min interval. Both the complexes show a reactivity pattern very similar to each other (Figure 11). Control experiments were performed using  $Co(ClO_4)_2 \cdot 6H_2O$  and 100 equiv of DTBCH<sub>2</sub>, where no change was observed in absorption intensity even after 1 d.

**Oxidation in MeOH.** The change in spectral behavior upon treatment with 3,5-DTBCH<sub>2</sub> has been shown in Figures 11 a and 11 b and the oxidation reaction was followed up to 50 min after addition of the substrate. Initially the absorption band for the complexes appeared at  $\approx 387 \text{ nm}$  which shifted to higher wavelength at  $\approx 401 \text{ nm}$ , with the generation of a shoulder at 309 nm after addition of the substrate 3,5-DTBCH<sub>2</sub>. With time, the intensity of the former peak gradually increases whereas the shoulder peak gradually disappears with progress of the reaction. The appearance and disappearance of the shoulder at 309 nm can be explained by taking into consideration the initial formation of *catalyst-substrate adduct*, which decomposes with time upon generation of 3,5-DTBQ.<sup>[37]</sup>

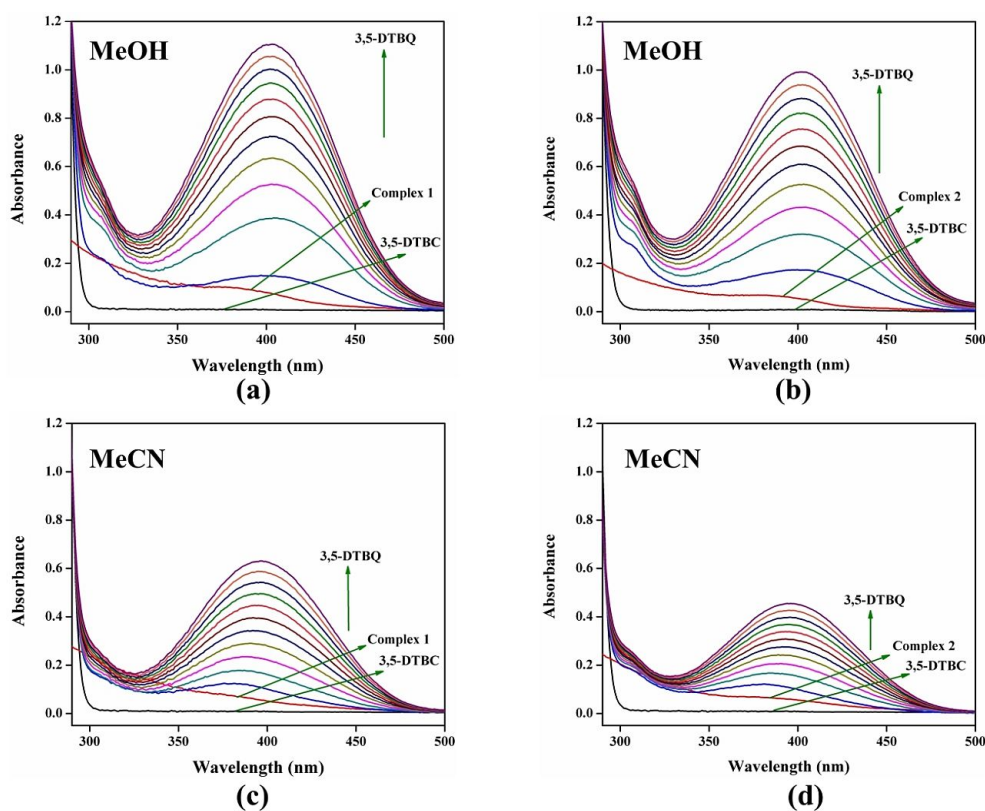


**Figure 11.** Time dependent UV-vis spectral changes for Complexes **1** and **2** (conc.  $\approx 1 \times 10^{-5} \text{ mol L}^{-1}$ ) upon addition of excess of (100 fold) 3,5-DTBCH<sub>2</sub> (conc.  $\approx 1 \times 10^{-3} \text{ mol L}^{-1}$ ) in MeOH (a and b) and in MeCN (c and d) at 298 K.

**Oxidation in MeCN.** The catalytic oxidizing power of **1** and **2** in air was studied and compared in MeCN medium to identify the solvent effect in the oxidation process. Upon treatment of **1** and **2**, having an absorption maximum at 380 nm, with 100 equivalents of DTBCH<sub>2</sub>, the peaks were blue shifted to ≈382 nm and ≈388 nm and the intensity increases with time identifying both as catalytically active compounds giving reactive fragments for the aerobic oxidation of DTBCH<sub>2</sub> (Figures 11c and 11d). The oxidation reaction was followed up to 50 min after addition of the substrate using UV-vis spectrophotometry. With progress of the reaction the peaks were shifted to higher wavelength with increase in intensity and become stabilized at 396 nm. Similar to the MeOH case, a shoulder appeared at ≈308 nm which gradually disappeared with the advancement of the reaction.

**Kinetic Study for Catechol Oxidation in MeOH and MeCN.** The kinetic behavior for the conversion of 3,5-DTBCH<sub>2</sub> to 3,5-DTBQ by **1** and **2** were carried out by monitoring the strong quinone (3,5-DTBQ) absorption band in MeOH and MeCN as a function of time (Figures 12 and 13). In both the two cases, a fixed concentration (≈1×10<sup>-5</sup> mol L<sup>-1</sup>) of complex solution was treated with varying concentration of 3,5-DTBCH<sub>2</sub> (10 to 100 equivalents). For all the complex-substrate combinations

the formation of 3,5-DTBQ was monitored by UV-vis spectroscopy by recording the change in absorption intensity with time at 401 nm for MeOH and 396 nm for MeCN up to first 10 minutes of mixing. The reaction rates were calculated by initial rate method and were analyzed by Michaelis–Menten model of enzyme kinetics. Important kinetic parameters such as reaction rate ( $V_{max}$ ), the binding constant ( $K_M$ ) and catalytic rate constant ( $k_{cat}$ ) were extracted from the corresponding Lineweaver–Burk plots of  $1/V$  vs.  $1/[S]$  (Figure 12 and Figure 13 insets) for all the four cases and are listed in Table 3.

The observed kinetic parameters are comparable to those reported in the literature for species with Co...Co separations in our range.<sup>[38]</sup> The turnover number ( $k_{cat}$ ) is the maximum

**Table 3.** Kinetic parameters for the catalytic oxidation of 3,5-DTBCH<sub>2</sub> by **1** and **2** in MeOH and MeCN medium at 25 °C.

Complex	Solvent	$V_{max}$ [M s <sup>-1</sup> ]	$K_M$ [M]	$k_{cat}$ [h <sup>-1</sup> ]	$k_{cat}/K_M$ [s <sup>-1</sup> M <sup>-1</sup> ]
<b>1</b>	MeOH	$7.86 \times 10^{-7}$	$4.95 \times 10^{-4}$	283	158
<b>2</b>	MeOH	$5.95 \times 10^{-7}$	$4.24 \times 10^{-4}$	214	140
<b>1</b>	MeCN	$1.95 \times 10^{-7}$	$1.39 \times 10^{-4}$	70	140
<b>2</b>	MeCN	$1.41 \times 10^{-7}$	$3.02 \times 10^{-4}$	51	47

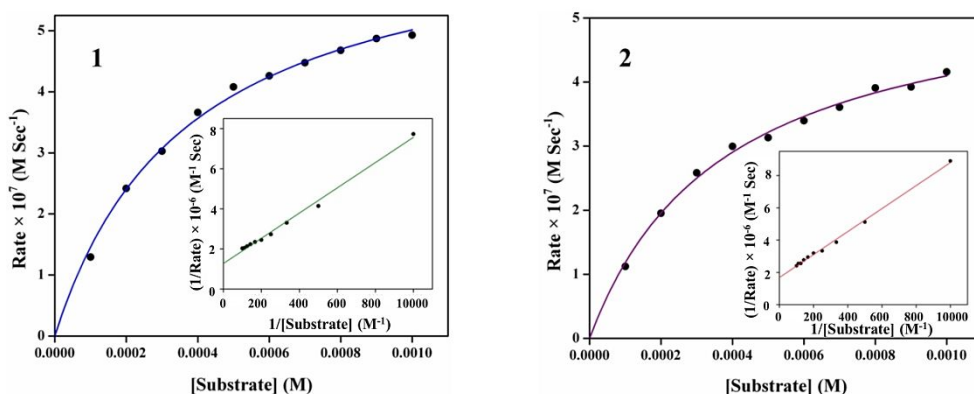


**Figure 12.** Dependence of the reaction rates on the substrate concentration for the oxidation of 3,5-DTBCH<sub>2</sub> catalyzed by complexes **1** and **2** in MeOH. The Lineweaver–Burk plots (inset).

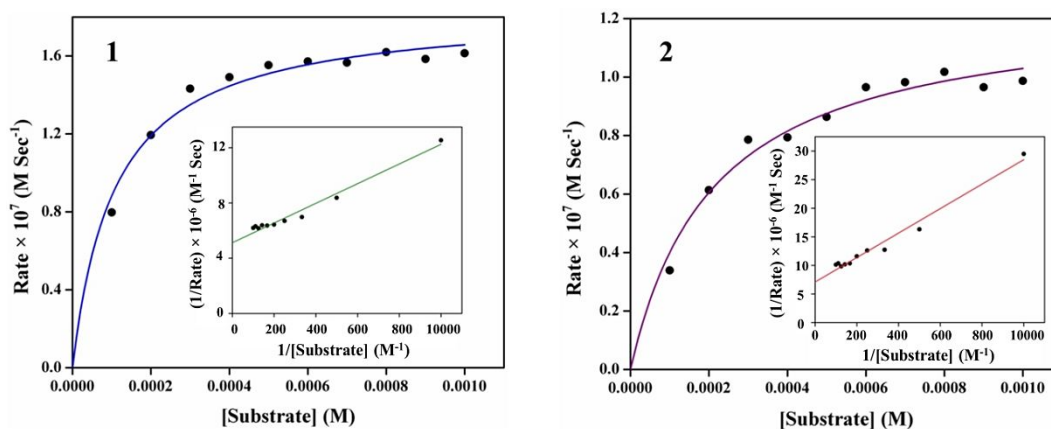


**Figure 13.** Dependence of the reaction rates on the substrate concentration for the oxidation of 3,5-DTBCH<sub>2</sub> catalyzed by complexes **1** and **2** in MeCN. The Lineweaver–Burk plots (inset).

number of moles of the substrate that can be converted to product per mole of catalyst in unit time. Determination of turnover number ( $k_{\text{cat}}$ ) in the present case is important to recognize the ability of the  $\{\text{Co}_2\}$  fragments in solution to catalyze the oxidation reaction. Spectrophotometric detection of  $\text{H}_2\text{O}_2$  based on the  $\text{I}_3^-$  anion formation and its identification as triiodide molybdate complex was important to propose the course of oxidation reaction. A comparison of  $k_{\text{cat}}$  values of **1–2** with previously reported cobalt complexes is given in Table S9 in Supporting Information.

**Mass Spectroscopic Analysis for the Fragments in Solution.** To identify the nature of the fragments present in the two solvents used in this study and their involvement in the catalytic process, we scrutinized corresponding mass spectral patterns of **1** and **2** in MeOH and MeCN solutions, respectively, in absence and presence of 3,5-DTBCH<sub>2</sub>.

**Complex 1.** The HRMS data for **1** in MeOH showed peaks (Figure S3 in Supporting Information) at  $m/z=371.1479$  corresponding to the protonated ligand  $\{\text{H}_3\text{L-H}\}^+$  ( $\text{C}_{17}\text{H}_{27}\text{N}_2\text{O}_3\text{S}_2$ ; Calcd 371.1463). Another peak at  $m/z=241.9857$  of high intensity is due to the fragment  $\{\text{Co}_2(\mu\text{-L})\}^{2+}$  ( $\text{C}_{17}\text{H}_{22}\text{Co}_2\text{N}_2\text{O}_3\text{S}_2$ ; Calcd 241.9863) while the peaks at  $m/z=545.0029$  and 560.9990 of lower intensity arise from the fragments  $\{\text{Co}_2(\mu\text{-L})(\text{CH}_3\text{COO})\text{-H}\}^+$  ( $\text{C}_{19}\text{H}_{27}\text{Co}_2\text{N}_2\text{O}_5\text{S}_2$ ; Calcd 545.0025) and  $\{\text{Co}_2(\mu\text{-L})(\text{CH}_3\text{COO})(\text{OH})\}^+$  ( $\text{C}_{19}\text{H}_{27}\text{Co}_2\text{N}_2\text{O}_6\text{S}_2$ ; Calcd 560.9975). Mixing of 3,5-DTBCH<sub>2</sub> and **1** in a molar ratio of 100:1 in MeOH resulted a peak (Figure S4 in Supporting Information) at  $m/z=705.4401$  for the catalyst and partially oxidized substrate adduct  $\{\text{Co}_2(\mu\text{-L})(\text{DTSQ})\}^+$  ( $\text{C}_{31}\text{H}_{43}\text{Co}_2\text{N}_2\text{O}_5\text{S}_2$ ; Calcd 705.1277). Whereas presence of  $\{\text{3,5-DTBQ-Na}\}^+$  and  $\{\{\text{3,5-DTBQ}\}_2\text{-Na}\}^+$  were diagnosed from the peaks at  $m/z=243.1371$  and 463.2823.

In MeCN, **1** provided peak (Figure S5 in Supporting Information) at  $m/z=371.1485$  for the protonated ligand ( $\text{C}_{17}\text{H}_{27}\text{N}_2\text{O}_3\text{S}_2$ ; Calcd 371.1463). A peak of considerable intensity at  $m/z=241.9867$  is due to the dimeric fragment  $\{\text{Co}_2(\mu\text{-L})\}^{2+}$  ( $\text{C}_{17}\text{H}_{22}\text{Co}_2\text{N}_2\text{O}_3\text{S}_2$ ; Calcd 241.9863) while the fragment  $\{\text{Co}_2(\mu\text{-L})(\text{CH}_3\text{COO})(\text{OH})\}^+$  ( $\text{C}_{19}\text{H}_{27}\text{Co}_2\text{N}_2\text{O}_6\text{S}_2$ ; Calcd 560.9975) documented a low intensity peak at  $m/z=560.9986$ . An additional peak at  $m/z=281.0037$ , of slightly lower intensity compared to the dimeric fragment, not present in MeOH medium can be most reasonably assigned to the monomeric fragment  $\{\text{Co}(\mu\text{-H}_2\text{L})(\text{CH}_3\text{COO})(\text{H}_2\text{O})_2\text{-K}\}^{2+}$  ( $\text{C}_{19}\text{H}_{32}\text{CoKN}_2\text{O}_7\text{S}_2$ ; Calcd 281.0305). In presence of 100 equivalent 3,5-DTBCH<sub>2</sub> in MeCN, **1** showed a low intensity peak (Figure S6 in Supporting Information) at  $m/z=705.4387$  for the dimeric intermediate  $\{\text{Co}_2(\mu\text{-L})(\text{DTSQ})\}^+$  ( $\text{C}_{31}\text{H}_{43}\text{Co}_2\text{N}_2\text{O}_5\text{S}_2$ ; Calcd 705.1277) following partial oxidation as obtained in the case of MeOH. One more peak at  $m/z=649.2134$  of comparatively higher intensity was assigned to a monomeric intermediate  $\{\text{Co}(\mu\text{-H}_2\text{L})(\text{DTSQ})\text{-H}\}^+$  ( $\text{C}_{31}\text{H}_{46}\text{CoN}_2\text{O}_5\text{S}_2$ ; Calcd 649.2175).

**Complex 2.** In MeOH very similar peaks, as found for **1**, were obtained at  $m/z=371.1461$  (protonated ligand  $\{\text{H}_3\text{L-H}\}^+$ ) and 241.9857 (fragment  $\{\text{Co}_2(\mu\text{-L})\}^{2+}$ ) for **2**. Other different peaks at  $m/z=559.0148$  and 575.0154 were assigned for fragments  $\{\text{Co}_2(\mu\text{-L})(\text{C}_2\text{H}_5\text{COO})\text{-H}\}^+$  ( $\text{C}_{20}\text{H}_{29}\text{Co}_2\text{N}_2\text{O}_5\text{S}_2$ ; Calcd 559.0182) and  $\{\text{Co}_2(\mu\text{-L})(\text{C}_2\text{H}_5\text{COO})(\text{OH})\}^+$  ( $\text{C}_{20}\text{H}_{29}\text{Co}_2\text{N}_2\text{O}_6\text{S}_2$ ; Calcd 575.0131) respectively (Figure S7 in Supporting Informa-

tion). The catalytically active fragment gave rise to the intermediate with the single electron oxidized substrate as  $\{\text{Co}_2(\mu\text{-L})(\text{DTSQ})\}^+$  ( $\text{C}_{31}\text{H}_{43}\text{Co}_2\text{N}_2\text{O}_5\text{S}_2$ ; Calcd 705.1277) at  $m/z=705.4434$  when 1:100 molar ratio mixture of **2** and 3,5-DTBCH<sub>2</sub> in MeOH was used for analysis. The peaks at  $m/z=243.1371$  and 463.2823 were assigned for  $\{\text{3,5-DTBQ-Na}\}^+$  and  $\{\{\text{3,5-DTBQ}\}_2\text{-Na}\}^+$  (Figure S8 in Supporting Information).

In MeCN medium exactly identical peaks were obtained at  $m/z=371.1445$  and 241.9867 for the different fragments ( $\{\text{H}_3\text{L-H}\}^+$  and  $\{\text{Co}_2(\mu\text{-L})\}^{2+}$ ) as mentioned earlier. The mass spectroscopic signature for the fragment  $\{\text{Co}_2(\mu\text{-L})(\text{C}_2\text{H}_5\text{COO})(\text{OH})\}^+$  ( $\text{C}_{20}\text{H}_{29}\text{Co}_2\text{N}_2\text{O}_6\text{S}_2$ ; Calcd 575.0131) appeared at  $m/z=575.0153$  in MeCN with an additional mononuclear fragment  $\{\text{Co}(\mu\text{-H}_2\text{L})(\text{C}_2\text{H}_5\text{COO})(\text{H}_2\text{O})_2\text{-K}\}^{2+}$  ( $\text{C}_{20}\text{H}_{34}\text{CoKN}_2\text{O}_7\text{S}_2$ ; Calcd 288.0383) at  $m/z=288.0119$  (Figure S9 in Supporting Information). As found in MeOH medium, the mixture of **2** and 3,5-DTBCH<sub>2</sub> in 1:100 molar ratio in MeCN medium resulted a low intensity peak at  $m/z=705.1401$  for  $\{\text{Co}_2(\mu\text{-L})(\text{DTSQ})\}^+$  ( $\text{C}_{31}\text{H}_{43}\text{Co}_2\text{N}_2\text{O}_5\text{S}_2$ ; Calcd 705.1277). At  $m/z=649.2227$ , another peak of comparatively higher intensity appeared due to  $\{\text{Co}(\mu\text{-H}_2\text{L})(\text{DTSQ})\text{-H}\}^+$  ( $\text{C}_{31}\text{H}_{46}\text{CoN}_2\text{O}_5\text{S}_2$ ; Calcd 649.2175) (Figure S10 in Supporting Information).

**EPR measurements.** To apprehend the involvement of Co<sup>II</sup> centers along with semiquinone based organic radical as intermediate species during the catechol oxidation, the X-band EPR spectral measurements were performed on **1** and **2** in MeOH and MeCN medium as well as in the presence of 3,5-DTBCH<sub>2</sub> at room temperature (Figure 14). Low-spin Co<sup>III</sup> ( $3d^6$ ) in an octahedral environment is diamagnetic and hence EPR inactive. Octahedral Co<sup>II</sup> ( $3d^7$ ) can exist in low spin state ( $S=1/2$ ) with  $t_{2g}^6e_g^1$  configuration and high spin state ( $S=3/2$ ) with  $t_{2g}^5e_g^2$  configuration. Low-spin paramagnetic Co<sup>II</sup> ions in  $C_{4v}$  or  $D_{4h}$  symmetry show EPR activity at room temperature due to the presence of longer spin lattice relaxation time and display small anisotropy in the  $g$  values. Whereas in the high-spin configuration, the Co<sup>II</sup> ions provide EPR signals only at very low temperatures with large anisotropy in the  $g$ -tensor due to short spin lattice relaxation time as a result of large orbital contribution towards the ground state magnetic moment.<sup>[12]</sup> Absence of any signal in the spectra of **1** and **2** in MeOH and MeCN solutions at room temperature was consistent with the presence of only ligand bound Co<sup>III</sup> fragments. In the presence of 100 equivalents of 3,5-DTBCH<sub>2</sub>, the MeOH solutions of **1** and **2** showed a sharp signal at  $g=2.0023$  indicating at the formation of semiquinone radical during the oxidation process. The signal was doubly split due to coupling with a single proton, positioning the lone electron on C4 of the benzene ring. A hyperfine structure of fifteen lines (one or more lines were obscured by strong radical signal) also appeared on both sides of the radical signal with  $g_{\text{iso}}=2.0006$  and  $A_{\text{iso}}=11$  gauss clearly indicating at the formation of Co<sup>II</sup> species by reduction of Co<sup>III</sup> during the catalytic cycle. Generally, the interaction of an unpaired electron on Co<sup>II</sup> with a nuclear spin of  $I=7/2$  (<sup>59</sup>Co,  $I=7/2$ , 100% natural abundance) should give rise to an eight line spectra. The appearance of fifteen line signal was due to the additional interaction with an adjacent cobalt nucleus through bridging phenoxido oxygen. The appearance of this

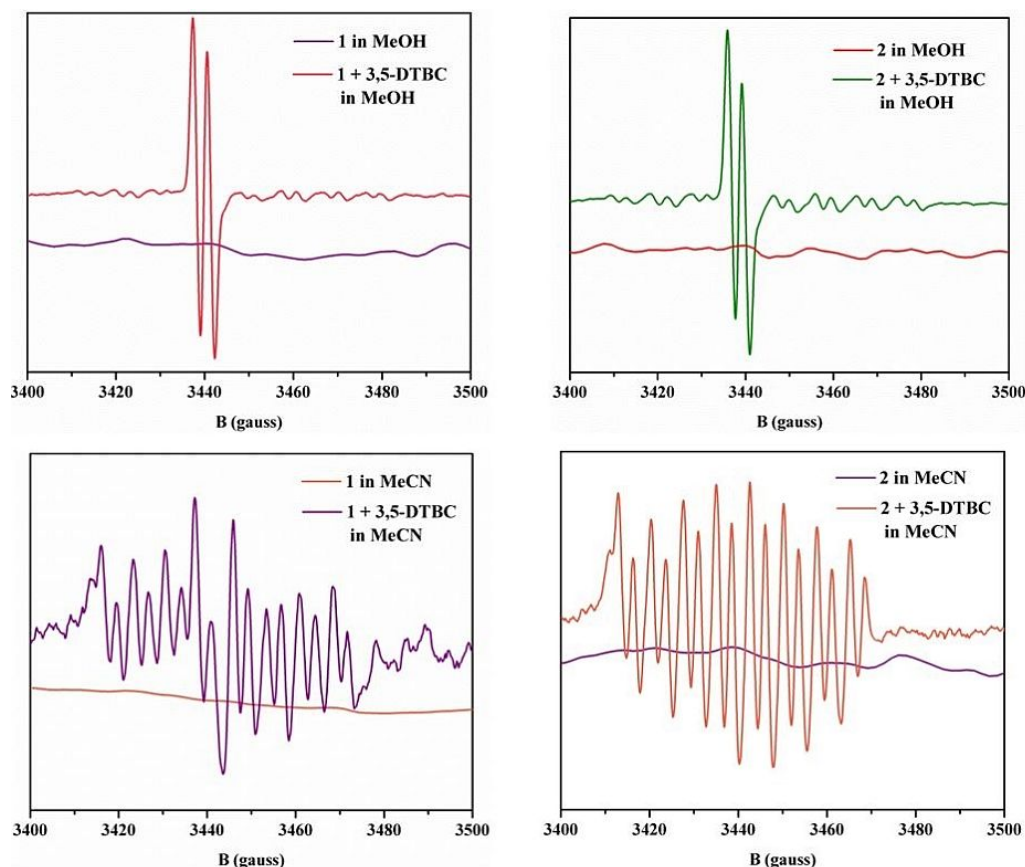


Figure 14. EPR spectra of 1 (left) and 2 (right) in MeCN and MeOH, respectively, and in the presence of 3,5-DTBC<sub>2</sub> at 298 K.

signal at room temperature suggests the generation of Co<sup>II</sup> ion in a *low-spin* state.

In MeCN, the spectra of 1 and 2 in presence of 100 equivalents of 3,5-DTBC<sub>2</sub> showed no representative signal corresponding to the formation of organic radical intermediate. This might probably be due to the transient nature and very low concentration of the formed radical species in this solvent medium. Formation of *low-spin* Co<sup>II</sup> species was confirmed from the appearance of fifteen line signals with  $g_{iso}=2.0006$  and  $A_{iso}=11$  gauss at room temperature. Simulation of the

spectra for 1 and 2 in MeCN by taking into consideration two <sup>59</sup>Co nuclei,  $S=1/2$  (*low spin* Co<sup>II</sup>),  $g_{iso}=2.0022$ ,  $A_{iso}=11$  gauss and average line width of 0.17 mT reproduced the experimental spectrum well with regard to the signal positions (Figure 15).

**Proposed Mechanism of Oxidation.** Reduction of O<sub>2</sub> into H<sub>2</sub>O<sub>2</sub> is often proposed for the catalytic oxidation of catechol with {Cu<sub>2</sub>} fragments or discrete complex species. In the present case recognition of H<sub>2</sub>O<sub>2</sub> by spectroscopic detection of triiodide (I<sub>3</sub><sup>-</sup>) anion as triiodide molybdate complex at 352 nm

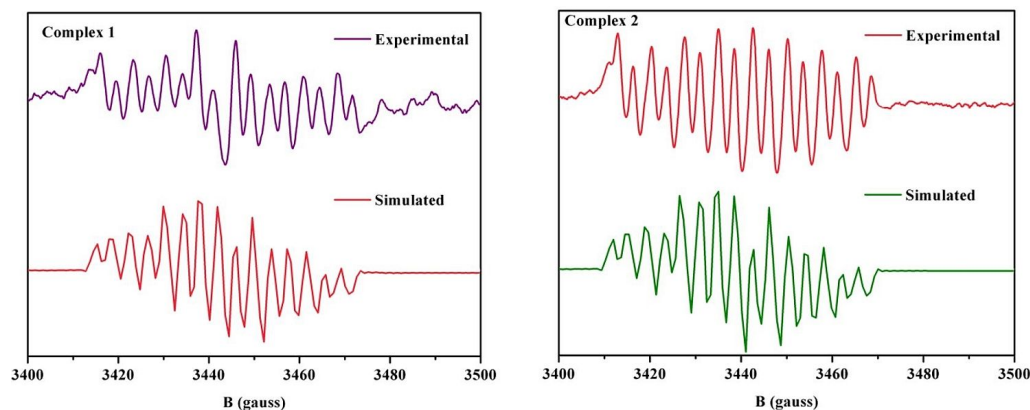


Figure 15. Experimental and simulated spectra for 1 (left) and 2 (right) in MeCN in the presence of 100 equivalent 3,5-DTBC<sub>2</sub>.

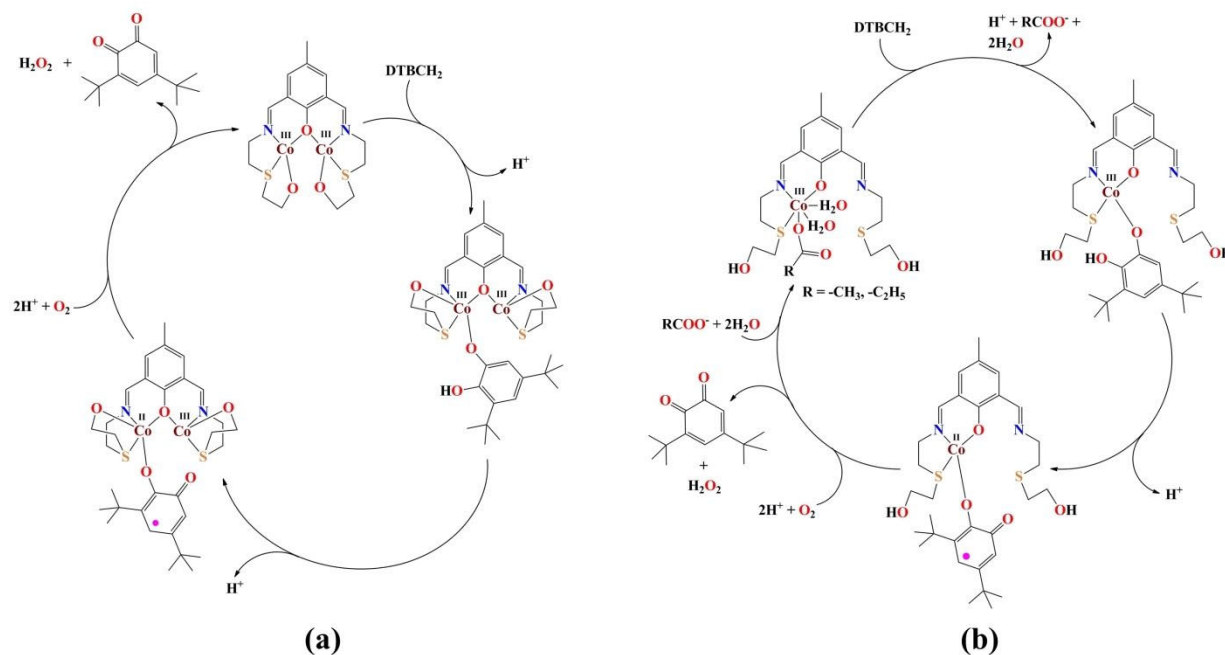
( $26\ 400\ \text{M}^{-1}\text{cm}^{-1}$ ), formed in the presence of  $\text{H}_2\text{O}_2$  from KI, points to the formation of  $\text{H}_2\text{O}_2$  during the catalytic cycle (Figure S11 in Supporting Information).<sup>[38]</sup> In contrast to the  $\{\text{Cu}_2\}$  based systems, the  $\text{Co}^{\text{II/III}}$  systems generally yield  $\text{H}_2\text{O}$  during oxidation.<sup>[39,40]</sup>

The HRMS and EPR analysis for **1** and **2** in absence and presence of 3,5-DTBCH<sub>2</sub> in MeOH and MeCN lead to a mechanistic pathway for the catalytic activity. In MeOH solution both **1** and **2** formed  $\{\text{Co}^{\text{III}}\text{Co}^{\text{III}}(\mu\text{-L})\}$  as the predominant fragment which serves as the active species for catalyzing the oxidation of 3,5-DTBCH<sub>2</sub> to 3,5-DTBQ. Upon addition of 3,5-DTBCH<sub>2</sub> the dimeric fragment possibly forms a 1:1 adduct with the substrate identified as the shoulder at 309 nm from UV-vis experiments. Herein we propose the coordination of 3,5-DTBCH<sub>2</sub> in its mono-deprotonated form as 3,5-DTBCH to only one of the  $\text{Co}^{\text{III}}$  centers due to the generation of  $\text{H}_2\text{O}_2$ .<sup>[20,41]</sup> One electron oxidation of the substrate accompanied by concomitant reduction of  $\text{Co}^{\text{III}}$  to  $\text{Co}^{\text{II}}$  results in the semiquinone radical bound intermediate species  $\{\text{Co}^{\text{II}}\text{Co}^{\text{III}}(\mu\text{-L})\}(\text{DTSQ})$  (Scheme 2a). Subsequent coordination of  $\text{O}_2$  to the  $\text{Co}^{\text{II}}$  center probably generates a  $\text{Co}^{\text{III}}$ -superoxo species. Loss of a second electron from the bound semiquinone to the  $\text{O}_2^-$  lead to the smooth formation of 3,5-DTBQ and  $\text{H}_2\text{O}_2$  regenerating the  $\{\text{Co}^{\text{III}}\text{Co}^{\text{III}}(\mu\text{-L})\}$  active species.

Interestingly, in MeCN the additional monomeric fragments,  $\{\text{Co}(\text{H}_2\text{L})(\text{CH}_3\text{COO})(\text{H}_2\text{O})_2\}$  and  $\{\text{Co}(\text{H}_2\text{L})(\text{C}_2\text{H}_5\text{COO})(\text{H}_2\text{O})_2\}$  could be detected for **1** and **2** respectively. While the dimeric species  $\{\text{Co}_2(\mu\text{-L})\}$  still predominates in solution, the monomers have a considerable abundance as is evident from the HRMS relative peak intensities. In the presence of 3,5-DTBCH<sub>2</sub> these form 1:1 adduct with the substrate followed by one electron oxidation giving rise to the intermediate  $\{\text{Co}^{\text{II}}(\text{H}_2\text{L})(\text{DTSQ})\}$  which greatly predominates over the dimeric intermediate  $\{\text{Co}^{\text{II}}\text{Co}^{\text{III}}(\text{L})(\text{DTSQ})\}$ .

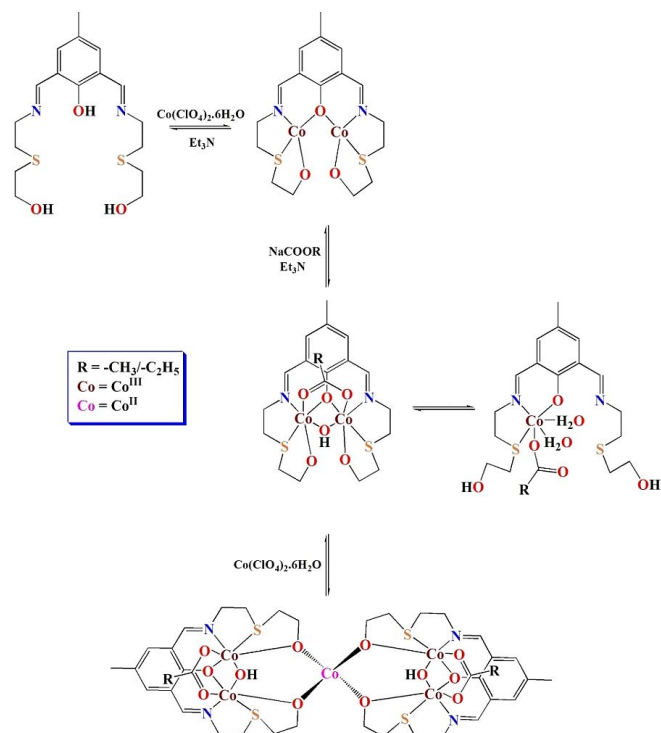
Hence, although the  $\{\text{Co}^{\text{III}}\text{Co}^{\text{III}}(\mu\text{-L})\}$  species still catalyzes the oxidation of the substrate, the major contribution comes from the  $\{\text{Co}^{\text{II}}(\text{H}_2\text{L})(\text{CH}_3\text{COO})(\text{H}_2\text{O})_2\}$  species (Scheme 2b). Subsequent oxidation of DTSQ and formation of  $\text{H}_2\text{O}_2$  takes place by a process similar to that described earlier. The kinetic experiments reveal that the  $k_{\text{cat}}$  values in MeCN are much lower compared to those in MeOH for both **1** and **2**. This can be attributed to the predominance of the monomeric species in the catalytic oxidation process in MeCN. The substrate 3,5-DTBCH preferentially binds to the monomeric fragment driven by less steric crowding and hydrogen bonding assistance from the dangling alcohol arm. The presence of a neighboring  $\text{Co}^{\text{III}}$  in the dimeric species facilitates the electron transfer from 3,5-DTBCH to the metal center. This is further supported by the fifteen line EPR spectrum suggesting considerable delocalization of the unpaired electron on the formed *low-spin*  $\text{Co}^{\text{II}}$  to the adjacent  $\text{Co}^{\text{III}}$  through the bridging phenoxido oxygen. Such assistance is not possible in case of the monomeric active species. The fifteen line spectrum observed in MeCN for **1** and **2** arises from a minor contribution of the dimeric active species in the oxidation process. These results demonstrate a probable strategy for enhancing the catalytic potency of a synthetic catalyst through introduction of a "spectator" metal ion center not involved in binding the substrate molecule. The observed slight difference in  $k_{\text{cat}}$  values between **1** and **2** in both MeOH and MeCN arises from the difference in concentration of the formed active fragments in solution.

**Probable Aggregation Pathway.** Structurally characterization of the single crystals of the end products established in this work and their disintegrations in solution visibly point to the presence of the building fragments necessary for the aggregation processes. Based on the types of the fragments



**Scheme 2.** Proposed catalytic pathway for **1** and **2** in (a) MeOH and MeCN (Minor contribution) and (b) MeCN (Major contribution). Only bonds to ligand and substrate has been shown, remaining sites are occupied by solvent molecules to fulfill octahedral coordination geometry of the metal ion centers.

found in the mass spectral analysis, it is possible to propose aggregation process from solution and during crystallization (Scheme 3). The identification of different fragments from HRMS measurements of **1** and **2** in MeCN solvent media revealed the involvement of these species in solution for the self-aggregation process during solid state isolation and crystallization.



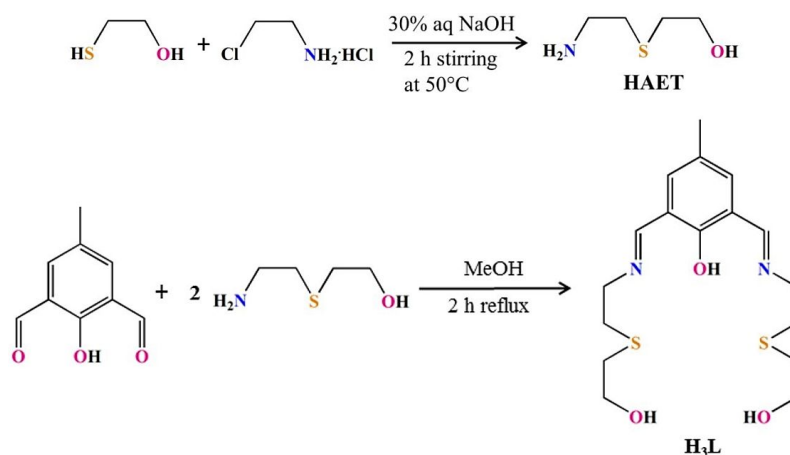
**Scheme 3.** Trapping of central cobalt ion through aggregation of dinuclear fragments in **1** and **2**.

Fragments like  $\{Co^{III}_2(\mu-L)\}$  and  $\{Co^{III}_2(\mu-L)(RCOO)(OH)\}$  in a step wise manner were utilized to gather the available ancillary bridges and the  $Co^{II}$  ion in central position from  $Co(ClO_4)_2 \cdot 6H_2O$  used during synthesis. The obtained fragments

$\{Co^{III}_2(\mu-L)(RCOO)(OH)\}$  behave as a O,O donor bidentate metal-ligand to trap the central  $Co^{II}$  ion for aggregation (Scheme 4).

## Conclusions

Two structurally unique  $[Co_3]$  complexes were synthesized to establish the usefulness of the chosen ligand system to bind four  $Co^{III}$  and one  $Co^{II}$  centers. Four thioether sulfur atom bound  $[Co_3]$  complexes described in this paper represented a new family of "mixed-valent-mixed-geometry" homometallic coordination aggregates. Evolution of the structural networks in **1** and **2** resulted from spontaneous assembly of diamagnetic  $\{Co^{III}_2(\mu-L)(RCOO)(OH)\}$  units (obtained from initial  $\{Co^{III}_2(\mu-L)\}$  units) through entrapment of a central  $Co^{II}$  ion which remained in distorted *pseudo-T<sub>d</sub>* coordination geometry. The amount of distortions from ideal *tetrahedral* geometry was determined from Houser's geometry index  $\tau_4$  values of 0.83 and 0.82, endorsing almost identical faintly compressed *tetrahedral* geometry in both cases. The ligand  $H_3L$  has been responsible for the coordination of two types of Co ions in these unusual structures. Both complexes **1** and **2** showed a relatively high easy-axis magnetic anisotropy ( $D/hc = -23.6$  (1) and  $-27.0$  cm<sup>-1</sup> (2)) and dynamic magnetic data confirmed that both the complexes behave as field-induced single-molecule magnets with spin reversal barrier  $U_{eff}/k_B = 30$  K (1) and 33 K (2), and relaxation time  $\tau_0 = 9.1 \times 10^{-8}$  s (1), and  $4.3 \times 10^{-8}$  s (2), respectively. The use of larger donor atom S lead to less variation in  $D$  and  $U_{eff}/k_B$  values in comparison to N used in our previous study. Theoretical calculations support the experimental findings. Thus an efficient methodology for varying the anisotropic parameters of a *pseudo tetrahedral*  $Co^{II}$  ion trapped within the constraint environments of diamagnetic  $Co^{III}$  based units have been established through simple variation of donor atoms. Interestingly the disintegration of **1** and **2** in solution gave rise to catalytically active molecular fragments suitable for the oxidation of the prototypical substrate 3,5-DTBC<sub>2</sub> with distinct solvent effects. Kinetic readings on the solvent-dependent oxidation reaction established that both the complexes exhibited lower  $k_{cat}$  values in MeCN compared to MeOH. ESI-MS (+ve) of



**Scheme 4.** Synthesis of HAET and  $H_3L$ .

the complexes in solution showed that dimeric  $\{\text{Co}^{\text{III}}_2(\mu\text{-L})\}$  type fragments were the key catalytic species in MeOH while in MeCN the predominant active species was monomeric  $\{\text{Co}^{\text{III}}(\text{H}_2\text{L})(\text{RCOO})(\text{H}_2\text{O})_2\}$  ( $\text{R}=\text{CH}_3$  (1),  $-\text{C}_2\text{H}_5$  (2)). A dimeric species was found to be more efficient at catalyzing the two electron oxidation of 3,5-DTBC $_2$  to 3,5-DTBQ as compared to a monomeric species due to the assistance provided by the adjacent  $\text{Co}^{\text{III}}$ .

## Experimental Section

**Materials.** The chemicals used here were obtained from the following sources: 2-mercaptoethanol, 2-chloroethylamine hydrochloride from Alfa Aesar, cobalt(II) carbonate, sodium acetate from SD Fine-Chem Ltd., India and  $\text{NEt}_3$  from Merck, India. Hydrated cobalt(II) perchlorate salt was freshly prepared by treating hydrated cobalt(II) carbonate with 1:1 aqueous  $\text{HClO}_4$  solution followed by crystallization. Sodium propionate was obtained by reacting propionic acid (11.1 g, 0.15 mol) with solid sodium hydroxide (6.0 g, 0.15 mol) in water, followed by concentration and crystallization on a water bath. 2,6-diformyl-4-methylphenol was prepared following a literature procedure with modification.<sup>[42]</sup> All other chemicals and solvents used in this work were reagent-grade and were used as received without further purification.

**Caution!** Metal complexes of organic ligands with perchlorate counter anions are potentially explosive. Although we did not face any problems with the reported compounds, it is advisable to prepare the materials in small amount and should be handled with extreme care.

**Synthetic Protocols. HAET (2-(2-aminoethylthio)ethanol).** The thioether incorporated amine alcohol was obtained from condensation of 2-mercaptoethanol and 2-chloroethylamine following a modified literature procedure.<sup>[43]</sup> 2-mercaptoethanol (0.780 g, 10 mmol) was added drop wise during 30 min to a 30% freshly prepared aq. NaOH solution (15 mL) with stirring and then heated to 50 °C. Next an aq. solution of 2-chloroethylamine hydrochloride (1.159 g, 10 mmol) was added drop wise to the above solution during a time period of 2 h. Finally the mixture was stirred for another 2 h period at 50 °C to give a pale yellow solution. The resulting solution was concentrated under reduced pressure, and then dissolved in absolute EtOH and filtered over glass frit to remove the precipitate. Removal of solvent from the filtrate under reduced pressure afforded HAET as a pale yellow liquid.  $^1\text{H}$  NMR (400 MHz,  $(\text{CD}_3)_2\text{SO}$ ):  $\delta=2.47\text{--}2.53$  (4H,  $-\text{CH}_2$ ), 2.63 (2H, methylene  $\text{CH}_2$  attached with N atom), 3.48 ppm (2H, methylene  $\text{CH}_2$  attached with O atom).  $^{13}\text{C}$  NMR (100 MHz,  $(\text{CD}_3)_2\text{SO}$ ):  $\delta=34.31$ , 35.99 (methylene C attached with S), 42.18 (methylene C attached with N atom), 61.43 ppm (methylene C attached with O atom).

**H<sub>3</sub>L (2,6-bis-[[2-(2-hydroxyethylthio)ethylimino]methyl]-4-methylphenol).** At room temperature, 2-(2-aminoethylthio)ethanol (1.21 g, 10 mmol) was added drop wise to 4-methyl-2,6-diformylphenol (0.820 g, 5 mmol) in MeOH (10 mL) with stirring and finally the whole mixture was refluxed for 2 h. Removal of solvent under vacuum yielded a yellow oily mass, which was characterized by FTIR and NMR spectroscopy. The oily product thus obtained was used directly for reactions with metal ion salts without further purification. FT-IR (KBr pellet):  $\tilde{\nu}=3368$  (br), 2918 (m), 1637(s), 1600 (w), 1458 (m), 1219 (w), 1045 (w), 1010 (w), 871 (w), 772  $\text{cm}^{-1}$  (s).  $^1\text{H}$  NMR (400 MHz,  $(\text{CD}_3)_2\text{SO}$ ):  $\delta=8.58$  (2H, imine-H), 7.49 (2H, Ar-H), 2.81–3.74 (8H, methylene  $\text{CH}_2$  attached with S atom), 3.52 (4H, methylene  $\text{CH}_2$  attached with O atom), 3.74 (4H, methylene  $\text{CH}_2$  at-

tached with N atom), 2.23 ppm (3H, methyl-H).  $^{13}\text{C}$  NMR (100 MHz,  $(\text{CD}_3)_2\text{SO}$ ):  $\delta=161.94$  (imine C), 159.98–121.27 (Ar C), 61.45 (methylene C attached to imine N), 59.64 (methylene C attached to OH group), 34.50–32.97 (methylene C attached to S), 20.35 ppm (methyl C).

**$[\text{Co}^{\text{III}}\text{Co}^{\text{III}}_4\text{L}_2(\mu\text{-OH})_2(\mu_{1,3}\text{-O}_2\text{CCH}_3)_2](\text{ClO}_4)_4\cdot\text{H}_2\text{O}$  (1).** To a stirred MeCN solution (15 mL) of H<sub>3</sub>L (approx. 0.37 g, 1 mmol) a MeCN solution (10 mL) of  $\text{Co}(\text{ClO}_4)_2\cdot 6\text{H}_2\text{O}$  (0.913 g, 2.5 mmol) was added. After 15 min of stirring, neat  $\text{NEt}_3$  (0.101 g, 1 mmol) was added followed by solid sodium acetate (0.164 g, 2 mmol). The final reaction mixture was stirred for 45 min and refluxed for 1 h. After cooling to room temperature the deep brown solution was filtered and kept in air for slow evaporation. After 18 days, brown colored block shaped single crystals of **1** were obtained. Yield: 0.535 g, (67% w.r.t. H<sub>3</sub>L). Anal Calcd. for  $\text{C}_{38}\text{H}_{56}\text{Cl}_4\text{Co}_5\text{N}_4\text{O}_{29}\text{S}_4$  (1597.54  $\text{g mol}^{-1}$ ): C, 28.57; H, 3.53; N, 3.51. Found: C, 28.71; H, 3.56; N, 3.49. Selected FT-IR bands: (KBr, vs.=very strong, br=broad, s=strong, m=medium, w=weak):  $\tilde{\nu}=3412$  (br), 1648 (m), 1576 (m), 1430 (m), 1090 (vs.), 626  $\text{cm}^{-1}$  (m). UV-vis spectra [ $\lambda_{\text{max}}$  nm ( $\epsilon$ ,  $\text{L mol}^{-1}\text{cm}^{-1}$ ): (MeCN solution) 620 (506), 598 (564), 556 (702), 382 (7300), 249 ( $54.9\times 10^3$ ).

**$[\text{Co}^{\text{III}}\text{Co}^{\text{III}}_4\text{L}_2(\mu\text{-OH})_2(\mu_{1,3}\text{-O}_2\text{CC}_2\text{H}_5)_2](\text{ClO}_4)_4\cdot\text{H}_2\text{O}$  (2).** Complex **2** was prepared following a similar procedure as described above for **1** using sodium propionate (0.192 g, 2 mmol) instead of sodium acetate. Brown colored block shaped single crystals suitable for X-ray analysis was obtained from the reaction mixture after 20 days. Yield: 0.478 g, (59% w.r.t. H<sub>3</sub>L). Anal Calcd. for  $\text{C}_{40}\text{H}_{56}\text{Cl}_4\text{Co}_5\text{N}_4\text{O}_{29}\text{S}_4$  (1621.56  $\text{g mol}^{-1}$ ): C, 29.63; H, 3.48; N, 3.45. Found: C, 29.72; H, 3.46; N, 3.46%. Selected FT-IR bands (KBr, s=strong, vs.=very strong, m=medium, br=broad):  $\tilde{\nu}=3421$ (br), 1647(m), 1577(m), 1459(m), 1090(vs.), 625  $\text{cm}^{-1}$  (m). UV/Vis spectra [ $\lambda_{\text{max}}$  nm ( $\epsilon$ ,  $\text{L mol}^{-1}\text{cm}^{-1}$ ): (MeCN solution): 619 (515), 596 (578), 557 (709), 378 (6300), 249 ( $46.9\times 10^3$ ).

**Physical Measurements.** Elemental analysis was performed by a PerkinElmer model 240C elemental analyzer. A Shimadzu UV 3100 UV/Vis-NIR spectrophotometer was used for electronic spectra and a PerkinElmer RX1 spectrometer for the FT-IR spectra. Powder X-ray diffraction (PXRD) patterns were measured on a BRUKER AXS X-ray diffractometer (40 kV, 20 mA) using  $\text{Cu-K}\alpha$  radiation ( $\lambda=1.5418$  Å) within 5–50° ( $2\theta$ ) range and a fixed-time counting of 4 s at 25 °C.

**X-ray crystallography.** X-ray diffraction data on appropriate single crystals of **1** and **2** were collected on a Bruker SMART APEX-II CCD X-ray diffractometer, equipped with a graphite monochromator and X-ray source of  $\text{Mo-K}\alpha$  radiation ( $\lambda=0.71073$  Å).  $\omega$ -scan at 293 K was used giving 5 s per frame. Space group determination, data integration and reduction were performed with XPREP and SAINT software.<sup>[44]</sup> The Structures were solved using the direct method through the SHELXS-2014<sup>[45]</sup> and refined with full-matrix least squares on  $F^2$  using the SHELXL (2014/7)<sup>[46]</sup> program package incorporated into WINGX system Version 2014.1.<sup>[47]</sup> Multiscan empirical absorption corrections were applied to the data using the program SADABS.<sup>[48]</sup> All non-hydrogen atoms were refined anisotropically. The H atoms were introduced in calculated positions and refined with fixed geometry and riding thermal parameters with respect to their carrier atoms. The locations of the heaviest atoms (Co) were determined easily, and the O, N, and C atoms were subsequently determined from the difference Fourier maps. Crystallographic diagrams were presented using DIAMOND software.<sup>[49]</sup> Information of concerned X-ray data collection and structure refinement of the compounds is summarized in Table 4 and in Table S1 in Supporting Information. CCDC 1857612 and 1857611 contain the supplementary crystallographic data for this paper.

**Table 4.** Crystal Data and Structure Refinement Details for **1** and **2**.

parameters	1	2
Formula	C <sub>38</sub> H <sub>56</sub> Cl <sub>4</sub> Co <sub>5</sub> N <sub>4</sub> O <sub>29</sub> S <sub>4</sub>	C <sub>40</sub> H <sub>56</sub> Cl <sub>4</sub> Co <sub>5</sub> N <sub>4</sub> O <sub>29</sub> S <sub>4</sub>
F.W. [g mol <sup>-1</sup> ]	1597.54	1621.56
crystal system	Orthorhombic	Monoclinic
space group	<i>Fdd2</i>	<i>P2<sub>1</sub>/c</i>
Crystal color	Red	Red
Crystal size [mm <sup>3</sup> ]	0.35 × 0.15 × 0.12	0.30 × 0.15 × 0.14
<i>a</i> [Å]	44.596(3)	23.278(5)
<i>b</i> [Å]	50.035(3)	12.529(3)
<i>c</i> [Å]	13.0237(8)	25.635(5)
$\alpha$ [deg]	90	90.00
$\beta$ [deg]	90	108.458(9)
$\gamma$ [deg]	90	90.00
<i>V</i> [Å <sup>3</sup> ]	29060(3)	7092(2)
<i>Z</i>	16	4
<i>D<sub>c</sub></i> [g cm <sup>-3</sup> ]	1.459	1.517
$\mu$ [mm <sup>-1</sup> ]	1.453	1.489
<i>F</i> (000)	12944	3284
<i>T</i> [K]	297(2)	296(2)
Total reflns	104086	84812
<i>R</i> (int)	0.1650	0.1154
Unique reflns	18145	14763
Observed reflns	11264	8858
Parameters	690	671
<i>R<sub>i</sub></i> ; <i>wR<sub>2</sub></i> ( <i>I</i> > 2 $\sigma$ ( <i>I</i> ))	0.0814, 0.2316	0.0998, 0.2940
GOF ( <i>F</i> <sup>2</sup> )	1.121	1.012
Largest diff peak and hole [e Å <sup>-3</sup> ]	1.756, -0.959	3.234, -1.745
CCDC No.	1857612	1857611

$R_1 = \sum(|F_o| - |F_c|) / \sum|F_o|$      $wR_2 = [\sum w(|F_o| - |F_c|)^2 / \sum w(F_o)^2]^{1/2}$      $w = 0.75 / (\sigma^2(F_o) + 0.0010F_o^2)$ .

These data are provided free of charge by The Cambridge Crystallographic Data Centre.

**Magnetic measurements.** The temperature-dependent ( $T = 1.9$ – $300$  K,  $B = 0.2$  T) and field-dependent ( $B = 0$ – $9$  T,  $T = 2, 5, 10$  K) magnetization measurements were performed on PPMS Dynacool (Quantum design Inc., San Diego, CA, USA) using a VSM option module. Dynamic magnetic properties were studied by measuring alternating current (AC) susceptibility on a MPMS XL-7 SQUID magnetometer in  $B_{dc} = 0$  and  $0.1$  T). The magnetic data were corrected for the diamagnetism of the constituent atoms and for the diamagnetism of the sample holder. The experimental data were fitted using the PHI program package.<sup>[26]</sup>

**Computational details.** All calculations were performed using the ORCA 4.0.0 program package on the X-ray crystal structures.<sup>[50]</sup> def2-TZVP basis set was employed on Co, N, O and S while def2-SVP basis set was employed on C and H.<sup>[51–53]</sup> State averaged complete active space self-consistent field (SA-CASSCF) calculations were performed on **1** and **2** using these basis sets with the active space comprising of seven d electrons of Co in five d orbitals i.e., CAS(7,5). 10 quartet and 40 doublet roots were computed using this active space in the CI (configuration interaction) step. *N*-electron valence perturbation theory (NEVPT2) was employed on the CASSCF wave function to account for the dynamic correlation. The zero-field splitting parameters (*D* and *E*) were calculated from both second-order perturbation theory and the modern effective Hamiltonian approach (EHA).<sup>[53]</sup> The spin-orbit coupling effects were incorporated by using a quasi-degenerate perturbation theory (QDPT) approach.

**Method for Kinetic Study.** The catechol oxidation behavior by the building fragments for **1** and **2** were examined in MeOH and

MeCN using 3,5-di-*tert*-butylcatechol (3,5-DTBCH<sub>2</sub>) as a model substrate. The oxidation of 3,5-DTBCH<sub>2</sub> to 3,5-di-*tert*-butylquinone (3,5-DTBQ) was followed on a Shimadzu UV 3100 UV-vis-NIR spectrophotometer. The reactions were monitored for the growth of quinone  $\lambda_{max}$  at  $\sim 400$  nm. Kinetic studies were performed in MeOH and MeCN medium, where the solutions of the complexes of constant concentrations ( $\sim 1.0 \times 10^{-5}$  M) were reacted with varying amounts of 3,5-DTBCH<sub>2</sub> (10 to 100 equiv) and the spectral changes were monitored with time at the  $\lambda_{max}$  of quinone. The data were treated using the initial rate method and the rate was obtained from the slope of the absorbance versus time plot. Kinetic analyses were executed following the Michaelis–Menten method, and important kinetic parameters were extracted from the Lineweaver–Burk plots.

**Detection of H<sub>2</sub>O<sub>2</sub>.** Generation of H<sub>2</sub>O<sub>2</sub> from O<sub>2</sub> of air during the oxidation of 3,5-DTBCH<sub>2</sub> was investigated by monitoring the growth of the characteristic absorption band for triiodide (I<sub>3</sub><sup>-</sup>) ion ( $\lambda_{max} = 353$  nm,  $\epsilon = 26000$  L mol<sup>-1</sup> cm<sup>-1</sup>).<sup>[54,55,56]</sup> The reaction mixture was acidified with H<sub>2</sub>SO<sub>4</sub> ( $1 \times 10^{-3}$  M) to pH 2 after 10 min of mixing to quench the reaction. The formed quinone was extracted with CH<sub>2</sub>Cl<sub>2</sub> and the aqueous layer was treated with 10% KI solution. The reaction can be represented as H<sub>2</sub>O<sub>2</sub> + 2I<sup>-</sup> + 2H<sup>+</sup> → 2H<sub>2</sub>O + I<sub>2</sub>. The I<sub>2</sub> liberated combines with excess iodide ions to form triiodide (I<sub>3</sub><sup>-</sup>) ions following the reaction I<sub>2</sub>(aq) + I<sup>-</sup> → I<sub>3</sub><sup>-</sup>. Addition of ammonium molybdate (3%) solution in a catalytic amount accelerates the reaction.<sup>[57]</sup> Blank experiments were also carried out as atmospheric oxygen can oxidize I<sup>-</sup> ions present in solution.

### Supporting Information

X-ray crystallographic data in CIF format, Figures S1–S11, Tables S1–S8. CCDC 1857612 and 1857611 contain the supplementary crystallographic data in CIF format for complexes **1** and **2**.

### Acknowledgements

M.D. and D.B. are grateful to IIT Kharagpur for their research fellowship. We are also thankful to DST, New Delhi, for providing the Single Crystal X-ray Diffractometer facility in the Department of Chemistry, IIT Kharagpur under FIST program. EPR facility by CRF, IIT Kharagpur is duly acknowledged. M.D. and D.B. are thankful to Mr. Sudipto Khamrui for his help with EPR measurements. Z.T. and J.V. thank the Ministry of Education, Youth and Sports of the Czech Republic (grant No. LO1305).

### Conflict of interest

The authors declare no conflict of interest.

**Keywords:** catecholase activity • cobalt • magnetic anisotropy • single-molecule magnets • thioether ligand

- [1] M. Sarkar, G. Aromí, J. Cano, V. Bertolasi, D. Ray, *Chem. Eur. J.* **2010**, *16*, 13825–13833.
- [2] D. Mandal, D. Ray, *Inorg. Chem. Commun.* **2007**, *10*, 1202–1205.
- [3] A. Ferguson, A. Parkin, J. Sanchez-Benitez, K. Kamenev, W. Wernsdorfer, M. Murrie, *Chem. Commun.* **2007**, 3473–3475.
- [4] S. Ziegenbalg, D. Hornig, H. Görls, W. Plass, *Inorg. Chem.* **2016**, *55*, 4047–4058.
- [5] S. Sottini, G. Poneti, S. Ciattini, N. Levesanos, E. Ferentinos, J. Krzystek, L. Sorace, P. Kyritsis, *Inorg. Chem.* **2016**, *55*, 9537–9548.

- [6] J. A. Sheikh, A. Clearfield, *Inorg. Chem.* **2016**, *55*, 8254–8256.
- [7] G. A. Craig, M. Murrie, *Chem. Soc. Rev.* **2015**, *44*, 2135–2147.
- [8] R.-C. Yang, D.-R. Wang, J.-L. Liu, Y.-F. Wang, W.-Q. Lin, J.-D. Leng, A.-J. Zhou, *Chem. Asian J.* **2019**, *14*, 1467–1471.
- [9] M. Murrie, *Chem. Soc. Rev.* **2010**, *39*, 1986–1995.
- [10] K. Chattopadhyay, M. J. H. Ojea, M. Sarkar, M. Murrie, G. Rajaraman, D. Ray, *Inorg. Chem.* **2018**, *57*, 13176–13187.
- [11] C. Gerdemann, C. Eicken, B. Krebs, *Acc. Chem. Res.* **2002**, *35*, 183–191.
- [12] S. K. Dey, A. Mukherjee, *New J. Chem.* **2014**, *38*, 4985–4995.
- [13] K. Chattopadhyay, G. A. Craig, M. J. H. Ojea, M. Pait, A. Kundu, J. Lee, M. Murrie, A. Frontera, D. Ray, *Inorg. Chem.* **2017**, *56*, 2639–2652.
- [14] T. Ghosh, J. Adhikary, P. Chakraborty, P. K. Sukul, M. S. Jana, T. K. Mondal, E. Zangrando, D. Das, *Dalton Trans.* **2014**, *43*, 841–852.
- [15] T. Singha Mahapatra, D. Basak, S. Chand, J. Lengyel, M. Shatruck, V. Bertolasi, D. Ray, *Dalton Trans.* **2016**, *45*, 13576–13589.
- [16] M. Mitra, P. Raghavaiah, R. Ghosh, *New J. Chem.* **2015**, *39*, 200–205.
- [17] R. Modak, Y. Sikdar, S. Mandal, S. Goswami, *Inorg. Chem. Commun.* **2013**, *37*, 193–196.
- [18] A. Hazari, L. K. Das, R. M. Kadam, A. Bauza, A. Frontera, A. Ghosh, *Dalton Trans.* **2015**, *44*, 3862–3876.
- [19] T. S. Mahapatra, Ph.D. thesis, Indian Institute of Technology Kharagpur, **2016**.
- [20] M. Das, Z. Afsan, D. Basak, F. Arjmand, D. Ray, *Dalton Trans.* **2019**, *48*, 1292–1313.
- [21] G. B. Deacon, R. J. Phillips, *Coord. Chem. Rev.* **1980**, *33*, 227–250.
- [22] K. Nakamoto, *Infrared and Raman Spectra of Inorganic and Coordination Compounds*, 4th ed., Wiley, New York, **1986**.
- [23] L. Yang, D. R. Powell, R. P. Houser, *Dalton Trans.* **2007**, 955–964.
- [24] N. E. Brese, M. O'Keefe, *Acta Crystallogr. Sect. B* **1991**, *47*, 192–197.
- [25] I. D. Brown, *The Chemical Bond in Inorganic Chemistry: The Bond Valence Model*, 2nd ed., Oxford University Press, **2002**.
- [26] N. F. Chilton, R. P. Anderson, L. D. Turner, A. Soncini, K. S. Murray, *J. Comput. Chem.* **2013**, *34*, 1164–1175.
- [27] M. Llunell, D. Casanova, J. Cirera, P. Alemany, S. Alvarez, SHAPE, ver. 2.1, Program for the Stereochemical Analysis of Molecular Fragments by Means of Continuous Shape Measures and Associated Tools, Departament de Química Física, Departament de Química Inorgànica, and Institut de Química Teòrica i Computacional—Universitat de Barcelona, Barcelona (Spain), **2013**.
- [28] R. Boča, J. Miklovič, J. Titiš, *Inorg. Chem.* **2014**, *53*, 2367–2369.
- [29] M. Atanasov, D. Aravena, E. Suturina, E. Bill, D. Maganas, F. Neese, *Coord. Chem. Rev.* **2015**, *289–290*, 177–214.
- [30] Y. Rechkemmer, F. D. Breitgoff, M. van der Meer, M. Atanasov, M. Haki, M. Orlita, P. Neugebauer, F. Neese, B. Sarkar, J. van Slageren, *Nat. Commun.* **2016**, *7*, 10467.
- [31] E. A. Suturina, D. Maganas, E. Bill, M. Atanasov, F. Neese, *Inorg. Chem.* **2015**, *54*, 9948–9961.
- [32] S. Gomez-Coca, E. Cremades, N. Aliaga-Alcalde, E. Ruiz, *J. Am. Chem. Soc.* **2013**, *135*, 7010–7018.
- [33] S. Vaidya, A. Upadhyay, S. K. Singh, T. Gupta, S. Tewary, S. K. Langley, J. P. Walsh, K. S. Murray, G. Rajaraman, M. Shanmugam, *Chem. Commun.* **2015**, *51*, 3739–3742.
- [34] S. Vaidya, S. K. Singh, P. Shukla, K. Ansari, G. Rajaraman, M. Shanmugam, *Chem. Eur. J.* **2017**, *23*, 9546–9559.
- [35] K. Peng, H. Wang, Z. Qin, G. T. Wijewickrama, M. Lu, Z. Wang, J. L. Bolton, G. R. J. Thatche, *ACS Chem. Biol.* **2009**, *4*, 1039–1049.
- [36] J. Mukherjee, R. Mukherjee, *Inorg. Chim. Acta* **2002**, *337*, 429–438.
- [37] K. S. Banu, T. Chattopadhyay, A. Banerjee, M. Mukherjee, S. Bhattacharya, G. K. Patra, E. Zangrando, D. Das, *Dalton Trans.* **2009**, 8755–8764.
- [38] C. Kormann, D. W. Bahnemann, M. R. Hoffmann, *Environ. Sci. Technol.* **1988**, *22*, 798–806.
- [39] L. I. Simándi, T. L. Simándi, *J. Chem. Soc. Dalton Trans.* **1998**, 3275–3279.
- [40] S. Tsuruya, S. Yanai, M. Masai, *Inorg. Chem.* **1986**, *25*, 141–146.
- [41] I. A. Koval, K. Selmecci, C. Belle, C. Philouze, E. S. Aman, I. G. Luneau, A. M. Schuitema, M. van Vliet, P. Gamez, O. Roubeau, M. Lüken, B. Krebs, M. Lutz, A. L. Spek, J.-L. Pierre, J. Reedijk, *Chem. Eur. J.* **2006**, *12*, 6138–6150.
- [42] R. R. Gagne, C. L. Spiro, T. J. Smith, C. A. Hamann, W. R. Thies, A. D. Shiemke, *J. Am. Chem. Soc.* **1981**, *103*, 4073–4081.
- [43] R. Veit, J.-J. Girerd, O. Kahn, F. Robert, Y. Jeannin, *Inorg. Chem.* **1986**, *25*, 4175–4180.
- [44] *Saint, Smart and XPREP*; Siemens Analytical X-ray Instruments Inc.: Madison, WI, **1995**.
- [45] G. M. Sheldrick, *SHELXS-2014, Program for Crystal Structure Solution*, University of Göttingen, **2014**.
- [46] G. M. Sheldrick, *Acta Crystallogr. Sect. A* **2008**, *64*, 112–122.
- [47] *WinGX-Version 2014.1*, L. J. Farrugia, *J. Appl. Crystallogr.* **2012**, *45*, 849–854.
- [48] G. M. Sheldrick, *SADABS: Software for Empirical Absorption Correction*; University of Göttingen, Institute für Anorganische Chemie der Universität, Göttingen, Germany, **1999–2003**.
- [49] DIAMOND, Visual Crystal Structure Information System, version 3.1; Crystal Impact, Bonn, Germany, **2004**.
- [50] F. Neese, *Wiley Interdiscip. Rev.: Comput. Mol. Sci.* **2012**, *2*, 73–78.
- [51] F. Weigend, R. Ahlrichs, *Phys. Chem. Chem. Phys.* **2005**, *7*, 3297–3305.
- [52] A. Hellweg, C. Hattig, S. Hofener, W. Klopper, *Theor. Chem. Acc.* **2007**, *117*, 587–597.
- [53] R. Maurice, R. Bastardis, C. de Graaf, N. Suaud, T. Mallah, N. Guihery, *J. Chem. Theory Comput.* **2009**, *5*, 2977–2984.
- [54] E. Monzani, L. Quinti, A. Perotti, L. Casella, M. Gullotti, L. Randaccio, S. Geremia, G. Nardin, P. Faleschini, G. Tabbi, *Inorg. Chem.* **1998**, *37*, 553–562.
- [55] E. Monzani, G. Battaini, A. Perotti, L. Casella, M. Gullotti, L. Santagostini, G. Nardin, L. Randaccio, S. Geremia, P. Zanello, G. Opromolla, *Inorg. Chem.* **1999**, *38*, 5359–5369.
- [56] J. Ackermann, F. Meyer, E. Kaifer, H. Pritzkow, *Chem. Eur. J.* **2002**, *8*, 247–258.
- [57] A. Neves, L. M. Rossi, A. J. Bortoluzzi, B. Szpoganicz, C. Wiezbicki, E. Schwingel, W. Haase, S. Ostrovsky, *Inorg. Chem.* **2002**, *41*, 1788–1794.

Manuscript received: August 9, 2019

Revised manuscript received: September 22, 2019

Accepted manuscript online: September 23, 2019

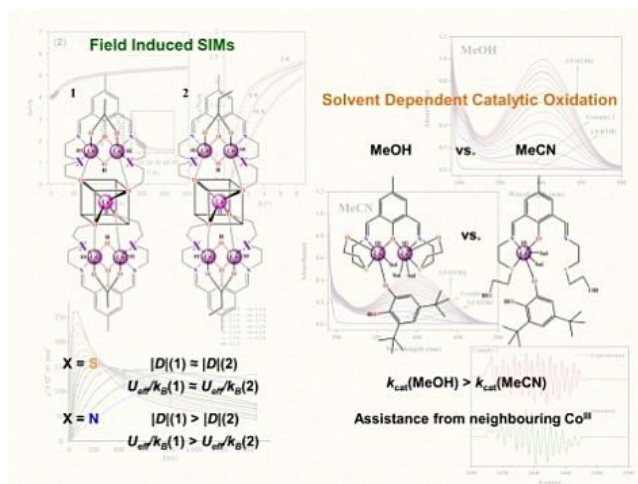
Version of record online: ■ ■ ■ 0000

## FULL PAPER

Manisha Das, Dipmalya Basak,  
Zdeněk Trávníček, Ján Vančo,  
Debashis Ray\*



Entrapment of a *Pseudo-Tetrahedral*  $\text{Co}^{\text{II}}$  Center by Thioether Sulfur Bound  $\{\text{Co}_2(\mu\text{-L})\}$  Fragments: Synthesis, Field-Induced Single-Ion Magnetism and Catechol Oxidase Mimicking Activity



The magnetic properties and catalytic activity of “mixed-valent-mixed-geometry”  $[\text{Co}_5]$  aggregates containing a *pseudo-tetrahedral*  $\text{Co}^{\text{II}}$  has been discussed. The use of the larger donor

atom S leads to less variation in  $D$  and  $U_{\text{eff}}/k_B$  values in comparison to N. Catalytically active fragments show catechol oxidase behavior with assistance from a “spectator”  $\text{Co}^{\text{III}}$  center.